

NASA TECHNICAL  
MEMORANDUM



N73-15817  
NASA TM X-2691

NASA TM X-2691

WAGE FILE  
COPY

ANALYSIS OF INTEGRAL  
LIFT-FAN ENGINE DYNAMICS

*by John R. Szuch*

*Lewis Research Center*

*Cleveland, Ohio 44135*

1. Report No. <b>NASA TM X-2691</b>	2. Government Accession No.	3. Recipient's Catalog No.	
4. Title and Subtitle <b>ANALYSIS OF INTEGRAL LIFT-FAN ENGINE DYNAMICS</b>		5. Report Date <b>January 1973</b>	
		6. Performing Organization Code	
7. Author(s) <b>John R. Szuch</b>		8. Performing Organization Report No. <b>E-7079</b>	
		10. Work Unit No. <b>764-72</b>	
9. Performing Organization Name and Address <b>Lewis Research Center National Aeronautics and Space Administration Cleveland, Ohio 44135</b>		11. Contract or Grant No.	
		13. Type of Report and Period Covered <b>Technical Memorandum</b>	
12. Sponsoring Agency Name and Address <b>National Aeronautics and Space Administration Washington, D.C. 20546</b>		14. Sponsoring Agency Code	
		15. Supplementary Notes	
16. Abstract An integral lift-fan engine being considered for VTOL applications was simulated using the hybrid computer. A contractor-proposed fuel control and a simple model of the roll dynamics of a hovering VTOL airplane were used in the simulation. Both steady-state and transient data were generated. The desired engine time constant of 0.20 second was achieved for thrust increments less than 10 percent of the design thrust. For roll angle demands less than 10°, roll angle overshoot was acceptable with more than 84 percent of the demand achieved in 1 second.			
17. Key Words (Suggested by Author(s)) <b>Engine dynamics; VTOL; Simulation; Hybrid computer; Turbofan; Control; Response; Time constant; Stability; Propulsion; Fuel control; Roll control; Thrust</b>		18. Distribution Statement <b>Unclassified - unlimited</b>	
19. Security Classif. (of this report) <b>Unclassified</b>	20. Security Classif. (of this page) <b>Unclassified</b>	21. No. of Pages <b>51</b>	22. Price* <b>\$3.00</b>

\* For sale by the National Technical Information Service, Springfield, Virginia 22151

# ANALYSIS OF INTEGRAL LIFT-FAN ENGINE DYNAMICS

by John R. Szuch

Lewis Research Center

## SUMMARY

This report describes the hybrid computer simulation of an integral lift-fan engine. This engine is being considered for use in future VTOL airplanes. The integral lift-fan engine is, in principle, a conventional two-spool turbofan engine with a high bypass ratio. A contractor-proposed fuel control system and a simple model of the roll dynamics of a hovering VTOL airplane were added to the simulation.

Both steady-state design and off-design data were generated using the simulation. Transient data were also generated to determine the effects of changes in the fuel control parameters, roll control parameters, and ambient temperature on the engine thrust and airplane roll angle response characteristics.

The results of the hybrid computer studies indicated that the integral engine concept lends promise of achieving the response goals of a VTOL propulsion system. Although not optimized, the nominal fuel control gains and acceleration fuel schedule resulted in engine time constants less than 0.2 second for standard-day thrust increments less than 10 percent of the design thrust. The determining factor in achieving a 0.20-second time constant for large thrust increments and/or hot-day conditions will be the tolerance of the turbines to transient overtemperatures.

With the deceleration schedule adjusted to give "mirror-image" thrust responses, the nominal roll control gains resulted in unsatisfactory roll angle responses. A 50-percent increase in the roll rate feedback gain was required to achieve a satisfactory roll angle response. For a  $10^{\circ}$  roll angle demand, the increased feedback gain resulted in a 13-percent overshoot in roll angle with 84 percent of the demand achieved in 1 second. For roll demands less than  $5^{\circ}$ , no overshoot was observed with 92 percent of the demand achieved in 1 second.

## INTRODUCTION

Advances in turbofan engine technology and aircraft design have now made low-noise, high-performance VTOL and STOL intercity transports possible (refs. 1 and 2). NASA

has been involved in both inhouse and contract studies of potential V/STOL propulsion systems (refs. 3 to 5). A number of proposed VTOL airplanes employ turbine-driven lift fans. The lift fan and drive turbine may be an integral part of the gas generator or may be remotely located. Figure 1 illustrates an integral lift-fan propulsion system (ref. 6). The self-contained drive engine eliminates the ducting (hence, weight) associated with remotely driven fan systems. The integral lift-fan engine is, in principle, a conventional two-spool turbfan engine with a high bypass ratio. The fan is shown with the core flow split off from the bypass flow. This geometry is attractive because it permits the hub

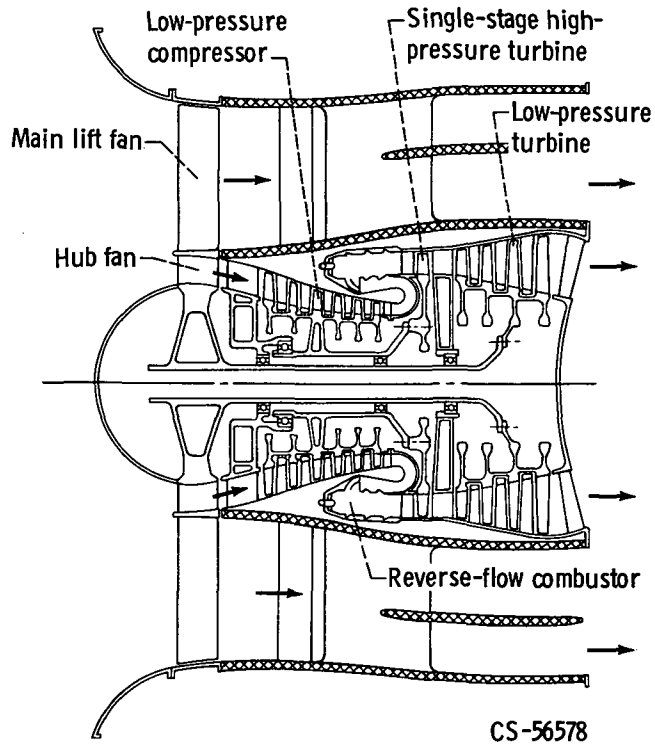


Figure 1. - Integral lift-fan engine.

section to operate at a lower pressure ratio than the main fan, thus permitting a smaller, lighter engine. The fan hub serves as a supercharger for the compressor. A reverse-flow combustor and a single-stage high-pressure turbine contribute to a short overall engine length.

This report describes the analytical simulation of the integral lift-fan engine. An existing general engine simulation program was used to implement the engine model on the hybrid (analog-digital) computer. A contractor-proposed fuel control system and a simple model of a VTOL airplane (in the roll mode) were also added to the simulation. The

assumption of "mirror-image" thrust responses for accelerations and decelerations allowed rolling moments to be generated with only one engine being simulated.

Both steady-state design and off-design data were generated using the simulation. Transient data were generated to determine (1) the effects of changes in the fuel control system on the engine thrust response characteristics, (2) the effects of changes in the ambient temperature on the engine response, (3) the effects of providing a turbine temperature limit in the fuel control on the engine response, (4) the acceleration and deceleration schedules of fuel flow required for fast response and mirror-image thrust characteristics, (5) the effects of thrust level and thrust increment on the engine "time constant," (6) the possible interactions between the airplane-engine control systems, (7) the effects of changes in the roll control system on the closed-loop response of the airplane, and (8) the effects of ambient temperature on the roll response characteristics.

## MATHEMATICAL MODEL

### Engine

Figure 2 shows, in block diagram form, the model assumed for the integral lift-fan engine. As mentioned previously, the engine contains two spools or drive systems. A high-pressure turbine drives the compressor while a low-pressure turbine drives the supercharger - lift-fan combination. The supercharger (core) and fan (bypass) flows are physically split. A portion of the compressor discharge air is bled off for turbine cooling. Schematically, some of the cooling air reenters the cycle downstream of the high-pressure turbine ( $\dot{w}_{bl1}$ ). The remainder of the cooling air ( $\dot{w}_{bl2}$ ) reenters the cycle downstream of the low pressure turbine. An overboard bleed flow ( $\dot{w}_{ovb}$ ) represents the flow lost from the cycle.

Except for the bleed flows, all the compressor discharge air enters the combustor where it reacts with the injected fuel to generate the high energy gas needed to drive the turbines. The discharge from the low pressure turbine is ducted to a converging nozzle which accelerates the flow and gives axial thrust. The discharge from the fan is also ducted to a converging nozzle which provides about 80 percent of the total engine thrust.

As indicated in figure 2, pressures and temperatures are computed in control volumes. In these volumes, storage of mass and energy occur (ref. 7). Pressure and temperature are assumed to be uniform in the volumes. The continuity equation, written for each volume, is

$$W = \int_0^t \left( \sum_1^{NN} \dot{w}_{in,j} - \sum_1^{MM} \dot{w}_{out,k} \right) dt + W_i \quad (1)$$

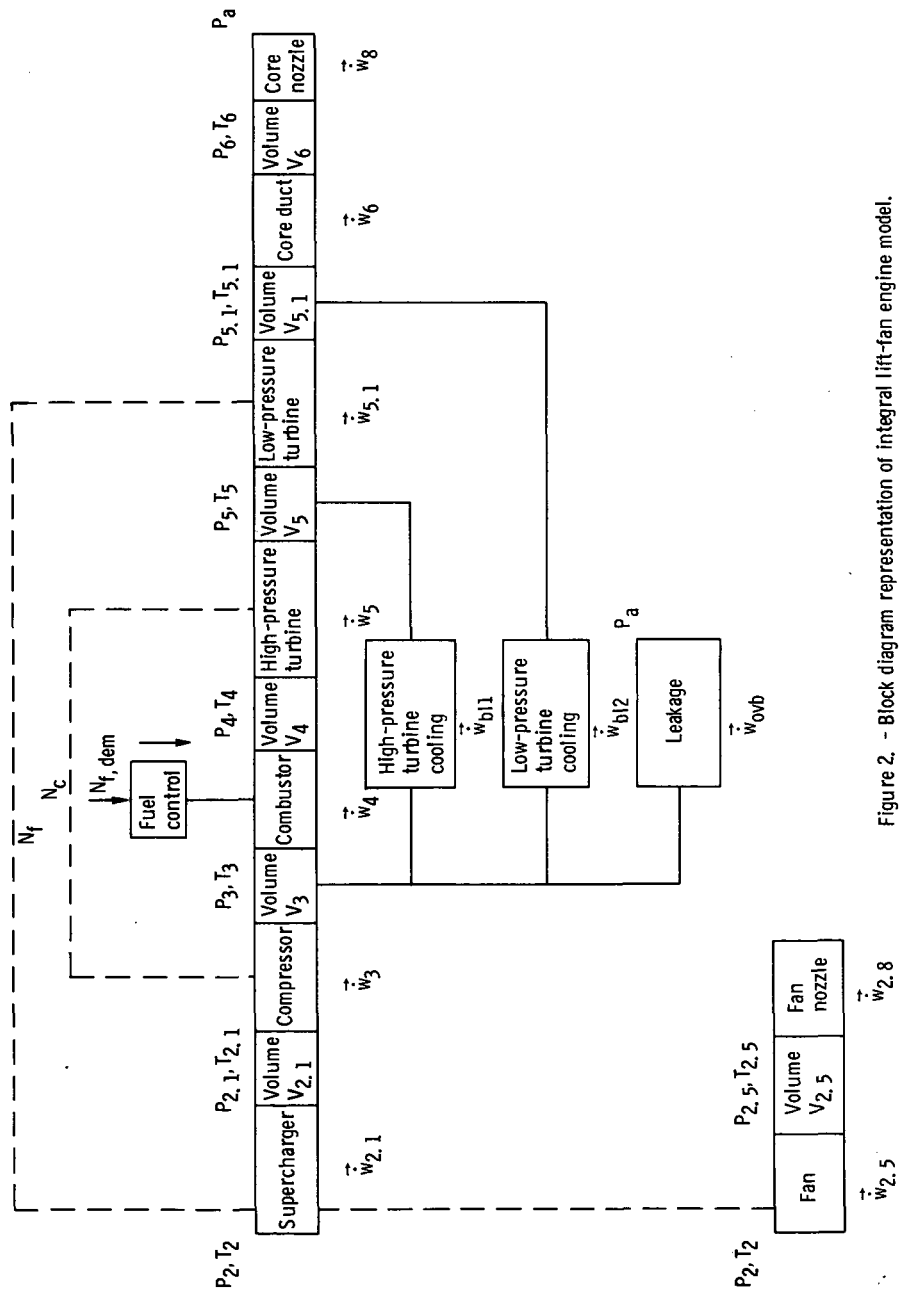


Figure 2. - Block diagram representation of integral lift-fan engine model.

(All symbols are defined in appendix A.) A summary of equations, as applied to specific components, is contained in appendix B. The energy equation, written for each volume, is

$$T = \int_0^t \frac{1}{W} \left\{ \frac{\sum_1^{NN} \dot{w}_{in,j} c_{p,in,j} T_{in,j}}{c_v} - T \left[ \sum_1^{NN} \dot{w}_{in,j} + (\gamma - 1) \sum_1^{MM} \dot{w}_{out,k} \right] \right\} dt + T_i \quad (2)$$

When the results from equations (1) and (2) are used, the pressure in the volume can be computed from

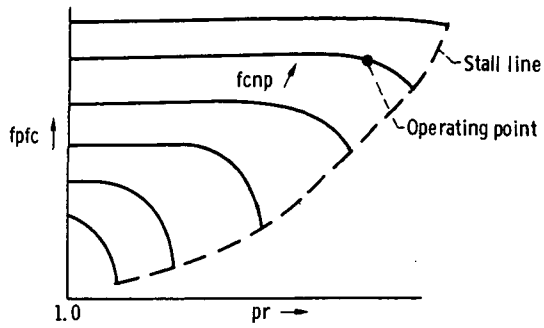
$$P = \frac{RWT}{V} \quad (3)$$

While the gas constant  $R$  is, in general, a function of the local fuel-air ratio, it was determined that the sensitivity of  $R$  to the fuel-air ratio could be neglected throughout the engine.

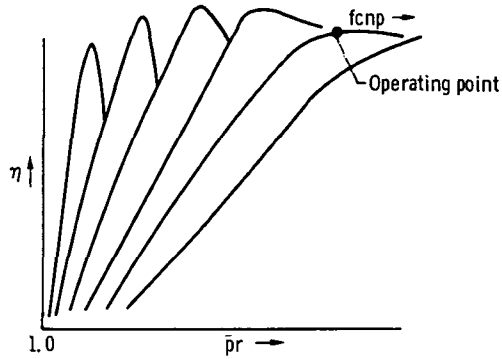
In addition to the intercomponent volumes, flows must be computed in the combustor and core duct. For these cases, the pressure drop across the control volume is assumed to be due to both friction and momentum effects. The momentum equation (ref. 8) is written for each control volume as

$$\dot{w} = \frac{Ag_c}{\lambda} \int_0^t (P_{in} - P_{out} - \lambda \dot{w}^2) dt + \dot{w}_i \quad (4)$$

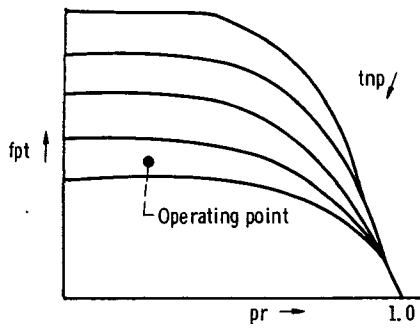
For the generalized hybrid computer program, fans, compressors, and turbines are represented by overall performance maps. Available component data must be converted to the forms shown in figure 3. Inputs to the component maps are pressure ratio and a speed parameter. For fans and compressors, the map outputs are a corrected flow parameter and adiabatic efficiency. For turbines, the outputs are a flow parameter and an enthalpy drop (work) parameter. A radial interpolation routine was used to generate the map outputs. For all components, the map outputs are used to compute flows, discharge temperatures, and torques. The computation of discharge temperature and torque, however, requires knowledge of the "average" values of  $c_p$  and  $\gamma$  in the component. These properties are assumed to be functions of temperature (the pressure dependence is



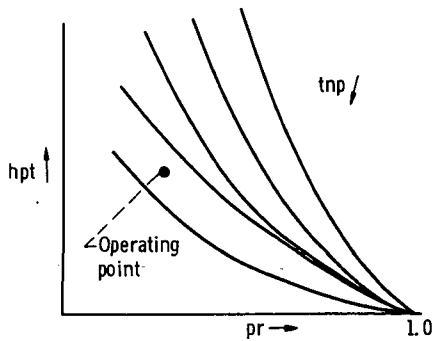
(a) Fan or compressor flow parameter map.



(b) Fan or compressor efficiency map.



(c) Turbine flow parameter map.



(d) Turbine enthalpy parameter map.

Figure 3. - Form of component performance data used in general engine simulation program.

neglected). Therefore, they vary throughout the component. For this reason, an interpolation constant  $\beta$  is adjusted for each component to match available cycle data; that is,

$$\bar{T} = \beta T_{in} + (1 - \beta) T_{out} \quad (5)$$

$$\bar{c}_p = \mathcal{F}\left(\bar{T}, \left(\frac{f}{a}\right)\right) \quad (6)$$

$$\bar{c}_v = \bar{c}_p - \frac{R}{J} \quad (7)$$

$$\bar{\gamma} = \frac{\bar{c}_p}{\bar{c}_v} \quad (8)$$

where  $(f/a)$  is the local fuel-air ratio.

After computing the fan, compressor, and turbine torques, the rotor speeds are determined by applying the principle of conservation of angular momentum; that is,

$$N = \frac{K_N}{I} \int_0^t \Delta L dt + N_i \quad (9)$$

For the integral lift-fan engine, the supercharger characteristics did not require mapping. Because of the very low pressure ratio involved, the efficiency could be assumed constant and the pressure ratio approximated by a linear function of rotor speed. The volume between the supercharger and compressor  $V_{2.1}$  was neglected, and the compressor flow was used to compute the supercharger torque. For the integral lift-fan engine, flows must be computed for both the core nozzle and fan discharge nozzle. All nozzles are assumed to be the convergent type and the flow processes throughout the nozzles are assumed to be isentropic. For a specified inlet pressure, there exists for each nozzle a critical back pressure (ref. 7) given by

$$P_{cr} = \left(\frac{2}{\gamma + 1}\right)^{\gamma/\gamma-1} P_{in} \quad (10)$$

If the back pressure on the nozzle is higher than the critical value, the flow is subsonic at the throat. For subsonic flow, the flow and thrust are given by

$$\dot{w} = P_{in} \sqrt{\frac{g_c}{RT_{in}}} A \left( \frac{P_{out}}{P_{in}} \right)^{1/\gamma} \sqrt{\frac{2\gamma}{(\gamma-1)} \left[ 1 - \left( \frac{P_{out}}{P_{in}} \right)^{\gamma-1/\gamma} \right]} \quad (11)$$

$$F = \sqrt{\frac{2J}{g_c}} \dot{w} \sqrt{c_p T_{in} \left[ 1 - \left( \frac{P_{out}}{P_{in}} \right)^{\gamma-1/\gamma} \right]} \quad (12)$$

If the back pressure is lower than the critical value, the flow at the throat is sonic or "choked." For this case, the flow and thrust are given by

$$\dot{w} = P_{in} \sqrt{\frac{g_c}{RT_{in}}} A \sqrt{\gamma \left( \frac{2}{\gamma+1} \right)^{\gamma+1/\gamma-1}} \quad (13)$$

$$F = \sqrt{\frac{2J}{g_c}} \dot{w} \sqrt{c_p T_{in} \left[ 1 - \left( \frac{P_{cr}}{P_{in}} \right)^{\gamma-1/\gamma} \right]} + A(P_{cr} - P_{out}) \quad (14)$$

Because of the computing equipment limitations, it was decided to neglect the effects of variable  $\gamma$  in the nozzle flow and thrust equations. A value of  $\gamma$  was selected to best match available cycle data. The turbine cooling bleeds and overboard bleed flow were computed using equation (13). The low back pressures allowed the flows to be computed without testing the associated pressure ratio.

## Fuel Control

Figure 4 shows a block diagram of a fuel control system proposed for the integral lift-fan engine. The function of the fuel control is to position a metering valve piston ( $x_v$ ) to provide the proper amount of fuel to the combustor so as to maintain fan speed  $N_f$  at a demanded value  $N_{f,dem}$ . Inputs to the fuel control system are fan speed  $N_f$ , compressor speed  $N_c$ , compressor discharge pressure  $P_3$ , demanded fan speed  $N_{f,dem}$ , and maximum allowable compressor speed  $N_{c,max}$ .

Transducer dynamics are included in the fuel control model. The two speed pickups are represented by 10-millisecond lags with gains of  $K_4$  and  $K_5$ . The pressure transducer is assumed to have a 30-millisecond time constant. The metering valve is repre-

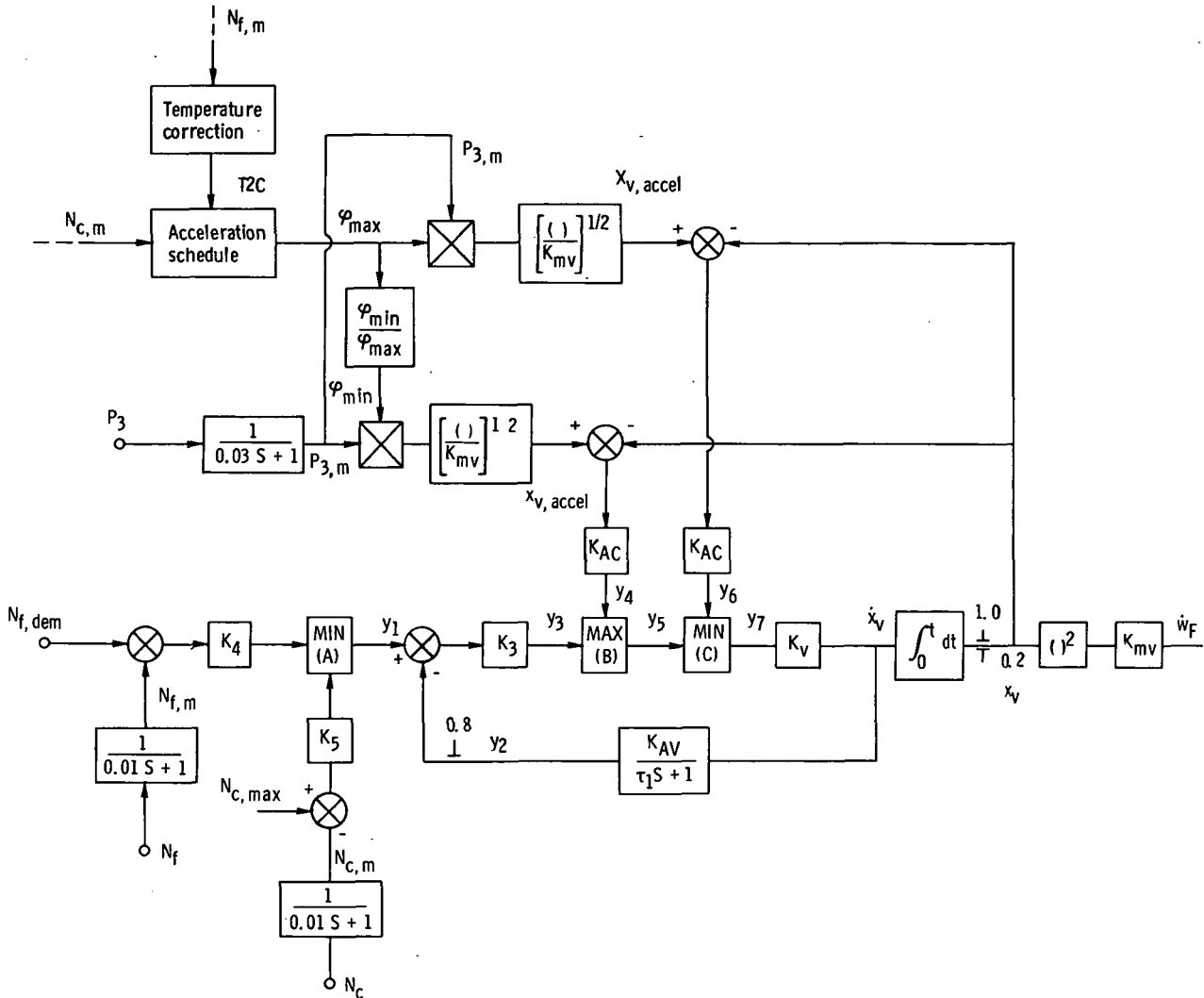


Figure 4 - Block diagram of contractor-proposed fuel control system for integral lift-fan engine.

sented by a gain  $K_V$ . An actuator gain  $K_{AC}$  relates the error in valve position to the rate of valve displacement  $\dot{x}_v$ . An actuator gain  $K_3$  relates a speed error to the rate of valve displacement. Valve position is the integral of  $\dot{x}_v$  and is limited between 0.2 and 1.0. Valve area is related to piston displacement by a square-law characteristic with the supplied fuel flow given by

$$\dot{w}_F = K_{mv} x_v^2 \quad (15)$$

Three MAX-MIN circuits are used to provide the logic needed to combine fast engine response with overspeed and overtemperature protection. The output of a MAX circuit is

equal to the largest of its inputs. Similarly, the output of a MIN circuit is equal to the smallest of its inputs. MIN circuit (A) is used to switch control to compressor speed if it approaches the maximum allowable speed  $N_{c, \max}$ . MAX circuit (B) and MIN circuit (C) determine whether valve position  $x_v$  is controlled by speed error or by the acceleration or deceleration fuel flow schedules. For example, in the initial stage of a deceleration, signals  $y_1$  and  $y_3$  are negative. MAX circuit (B) selects  $y_4$  for its output which results in closed loop control of  $x_v$  with  $x_{v, \text{decel}}$  as the commanded position. Later in the transient  $y_3$  will exceed  $y_4$  and the valve position will be controlled by the speed error.

The acceleration schedule, as shown, consists of a map of

$$\phi_{\max} = \left( \frac{\dot{w}_F}{P_3} \right)_{\text{accel}}$$

as a function of compressor speed  $N_c$  with a fan speed-sensitive correction factor T2C. The deceleration schedule  $\phi_{\min}$  is assumed to be equal to  $\phi_{\max}/2$ . The measured pressure  $P_{3, m}$  is used to multiply  $\phi_{\max}$  and  $\phi_{\min}$  to find the corresponding limits on fuel flow and valve position.

To increase the system damping, hence stability, rate feedback is used to control the metering valve. While the block diagram indicates actual measurement of  $\dot{x}_v$  with a feedback transfer function having a lag characteristic (i. e.,  $y_2 = K_{AV}/[(\tau_1 s + 1)] \dot{x}_v$ ), the actual feedback would probably be accomplished by passing a position signal  $x_v$  through a lead-lag network having the required frequency response characteristics. A summary of the equations describing the fuel control system is given in appendix B.

## Airplane Roll Control

Figure 5 shows an illustration of the simple VTOL airplane configuration assumed for this study. The selected VTOL airplane weighed  $W_{AP}$  at takeoff and used  $n_E$  lift engines ( $n_E/2$  to a side). The airplane had a roll moment of inertia of  $I_{AP}$ .

The lift engines were all at an equal moment arm of  $r_{AP}$  and were used for both lift and roll control. For roll simulations, all engines were assumed to respond identically on each side with the opposite engines responding in a mirror-image fashion. This assumption allows roll-mode simulation with only one engine being simulated. While not always achievable, the mirror-image characteristic would also be desirable from a fuel control implementation viewpoint.

Figure 6 shows a block diagram of the airplane roll control system. The inputs to the roll control system are the demanded roll angle  $\theta_{\text{dem}}$ , the measured roll angle  $\theta$ ,

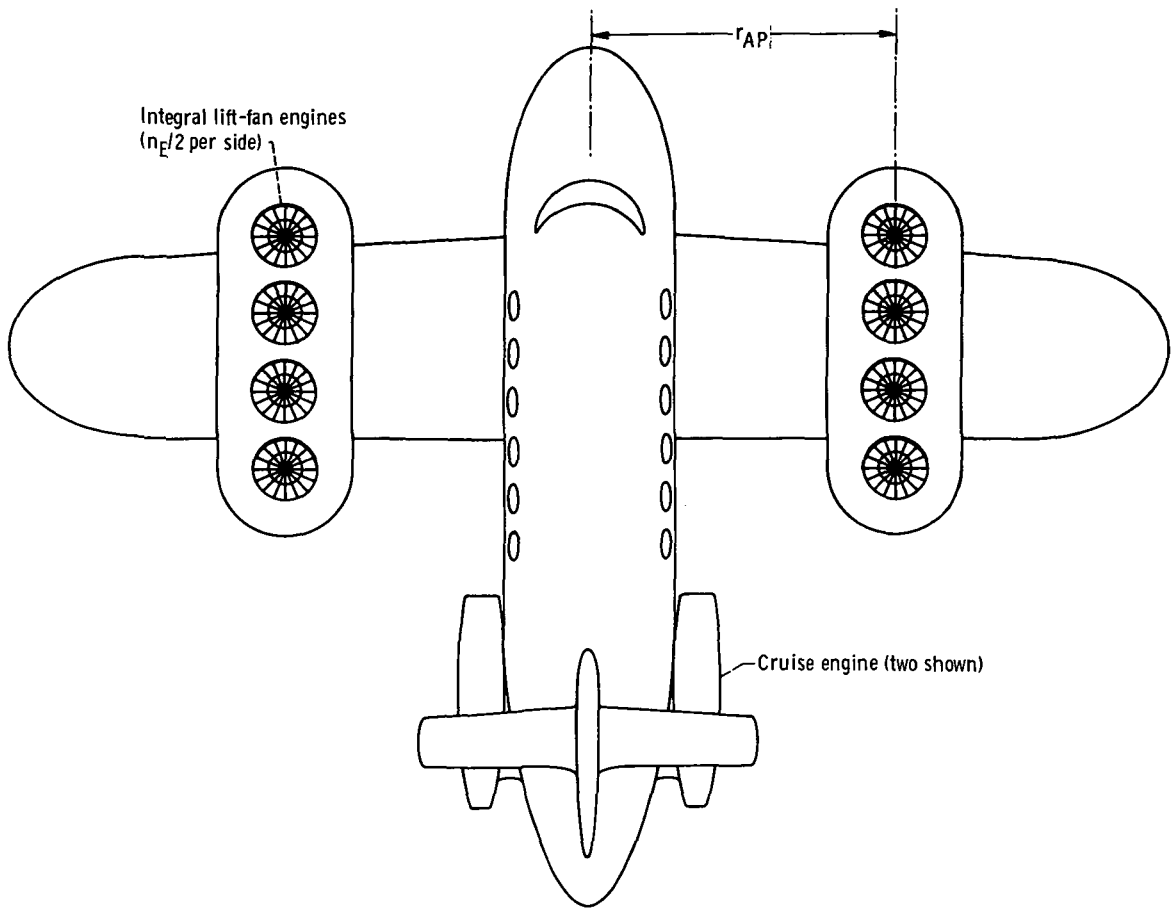


Figure 5. - Assumed VTOL airplane configuration.

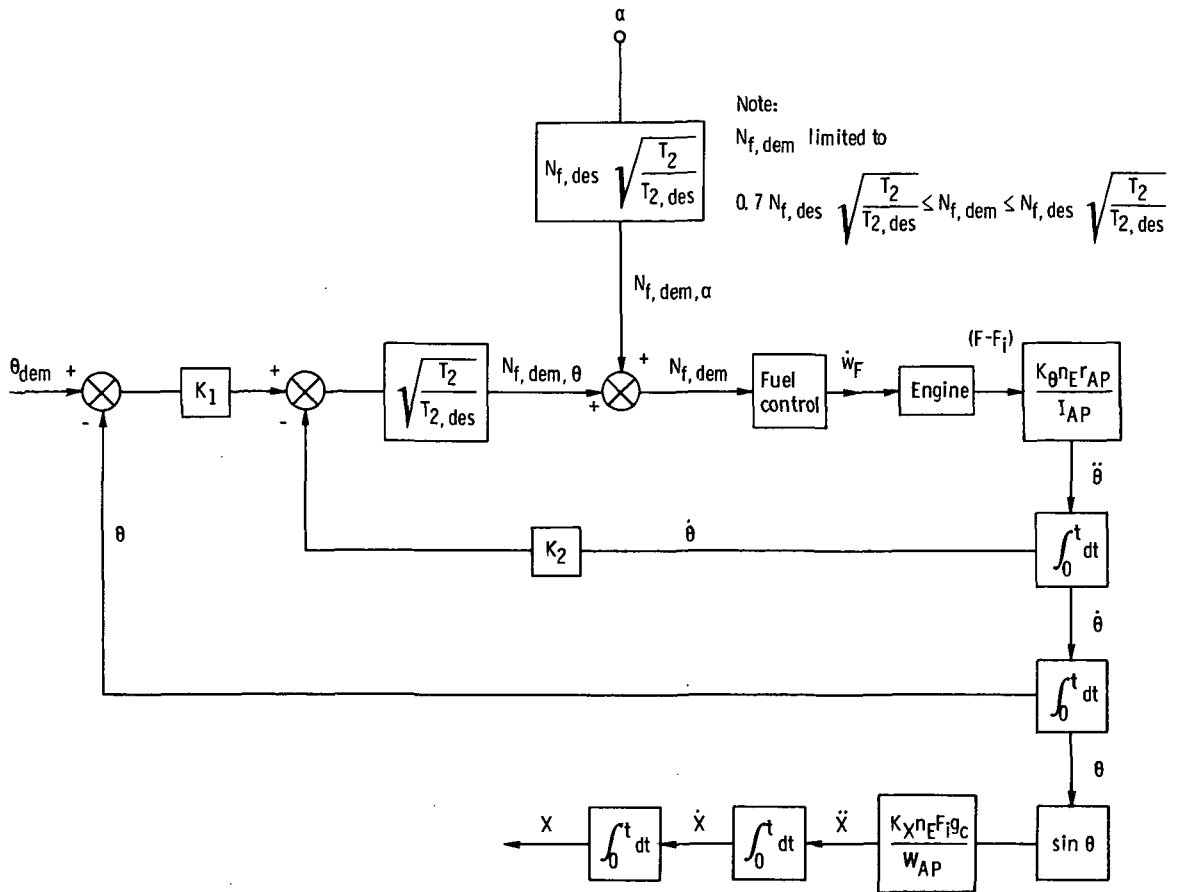


Figure 6. - Block diagram of integral engine VTOL airplane roll control.

and the measured roll rate  $\dot{\theta}$ . The angular roll rate is fed back to add damping to the closed-loop system. The input to the fuel control  $N_{f, dem}$  is the sum of the throttle demand  $N_{f, dem, \alpha}$  and the roll angle error demand  $N_{f, dem, \theta}$ . To prevent overspeeds and/or overtemperatures, the fuel control input was limited to  $N_{f, dem} \leq N_{f, 100}$  where  $N_{f, 100}$  is the fan speed at the design thrust. For this study, roll maneuvers were conducted at the takeoff thrust and the fuel control input was limited to  $N_{f, dem} \geq 0.7 N_{f, 100}$ . The limits would probably be temperature sensitive to account for changes in the ambient temperature. The fuel control generates the fuel flow  $\dot{w}_F$  to the engine which, in turn, generates the thrust (lift)  $F$ . The  $n_E/2$  engine pairs generate a rolling angular acceleration, which is given by

$$\ddot{\theta} = K_{\theta} \frac{n_E r_{AP}}{I_{AP}} (F - F_i) \quad (16)$$

where  $F_i$  is the engine thrust which results in a steady nonrolling condition. The angular roll rate and roll angle are determined by successive integrations of the angular acceleration. Both the roll angle and roll rate are fed back to the roll control system. The error between the demanded roll angle and the measured roll angle is multiplied by the gain  $K_1$ . The angular roll rate is multiplied by the gain  $K_2$  and subtracted from the amplified angle error. A temperature-sensitive gain is used to compensate for changes in the ambient temperature. Therefore, the roll error demand is given by

$$N_{f, \text{dem}, \theta} = \sqrt{\frac{T_2}{T_{2, \text{des}}}} \left[ K_1(\theta_{\text{dem}} - \theta) - K_2\dot{\theta} \right] \quad (17)$$

The roll angle results in a lateral acceleration of the airplane given by

$$\ddot{X} = K_X \frac{n_E F_i}{W_{AP}} g_c \sin \theta \quad (18)$$

For a hovering condition, the total thrust is equal to the airplane weight.

The lateral velocity and displacement are determined by successive integrations of the lateral acceleration. A summary of the equations describing the airplane roll control model is given in appendix B.

## COMPUTER PROGRAM

The integral lift-fan engine was simulated using an existing general engine program. The computer program allows simulation of either turbojet or turbofan engines while minimizing the required manpower and programming effort. The use of the hybrid computer combines the accuracy associated with a digital computer with the continuous integration and user monitoring associated with the analog computer.

The digital computer was used to (1) control the operation of the program, (2) perform the logic required to set up the integral engine configuration, (3) perform the function generation associated with the engine component models, and (4) perform most of the algebraic computations. The digital program was structured in subroutine form to minimize core storage requirements and to allow convenient program modification if required. The digital portion of the Lewis Research Center hybrid computer has 16 384 words of core storage. Floating point (real) numbers are represented by two 16-bit words. Scaled fractions (less than 1.0) are represented by a single 16-bit word. To minimize both the core requirements and computation time, the general engine program

was written using scaled-fraction digital computation.

The analog portion of the hybrid computer provided the integration (with respect to time) associated with the system dynamics. The analog computer was used to compute stored weights, temperatures, pressures, duct flows, and rotor speeds. The analog computer was also used to implement the fuel control and airplane roll control models. Conventional strip-chart recorders and X-Y plotters were used to monitor the transient behavior of selected engine-airplane variables.

For the integral lift-fan engine simulation, the analog portion of the program was time scaled (slowed down) by a factor of 100. This provided an acceptable ratio of digital cycle frequency to analog system frequencies and allowed the stepwise varying digital inputs to the analog to be treated in a continuous manner. The combination of the 100:1 time scaling and the digital cycle time of 43 milliseconds represents a 10:1 speedup in computation time when compared with all-digital simulation experiences.

## RESULTS

The integral lift-fan engine (figs. 1 and 2) was simulated on the hybrid computer. Engine design point data, together with selected amplitude and time-scale factors, were used to generate input data required by the general engine simulation program. The engine design point corresponds to hot-day (305.4 K, 549.7° R), maximum thrust conditions. Also put into the program were performance data for the eight engine component maps (two each for the fan, compressor, high-pressure, and low-pressure turbines).

### Steady-State Engine Operation

The hybrid computer simulation of the integral engine was operated at the hot-day design point. The temperature interpolation constants ( $\beta_f$ ,  $\beta_c$ ,  $\beta_b$ ,  $\beta_{t1}$  and  $\beta_{t2}$ ) were adjusted to achieve a steady-state cycle balance at the design point.

The resultant steady-state operating point differed from the design point by less than 0.8 percent for system pressures, 0.18 percent for system temperatures, 0.3 percent for system flows, 0.35 percent for rotor speeds, and 0.65 percent for engine thrust. By varying the throttle demand  $\alpha$  on the analog, the engine was throttled to the nominal takeoff condition (80 percent thrust) and selected engine variables were recorded. The ambient temperature  $T_2$  was then decreased to the standard-day temperature (288.2 K, 518.7° R). The throttle demand was adjusted to give the same takeoff and maximum thrust values. Table I lists computed engine variables at the takeoff and maximum thrust conditions for both standard and hot days. The table also presents the end conditions for a number of transients run during this program.

TABLE I. - STEADY-STATE COMPUTED ENGINE DATA

[All values specified as percent of design point.]

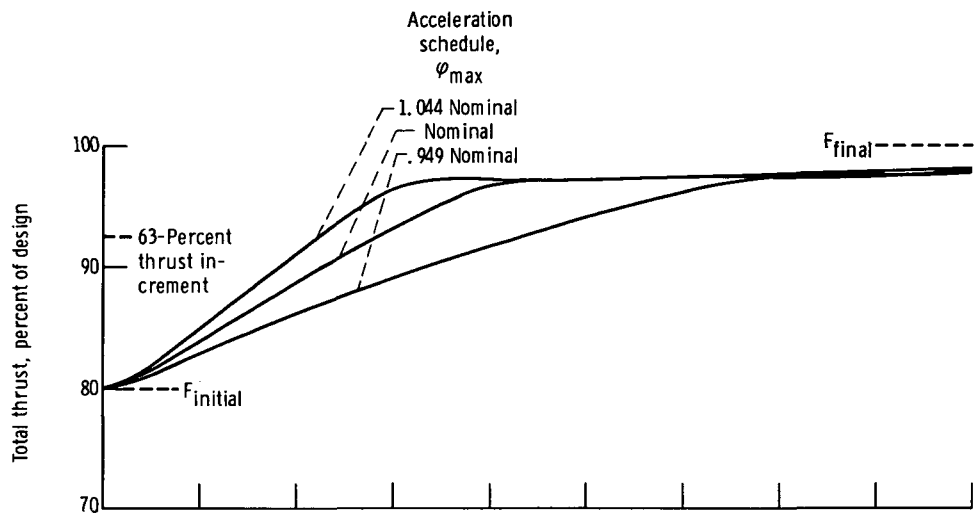
	Hot day		Standard day	
	Takeoff	Maximum thrust	Takeoff	Maximum thrust
Thrust	79.5	99.4	79.9	99.6
High-pressure turbine inlet temperature	92.1	99.9	87.7	95.6
Fan speed	89.4	100.3	87.2	97.6
Compressor speed	95.6	100.1	93.0	97.6

### Fuel Control - Engine Response

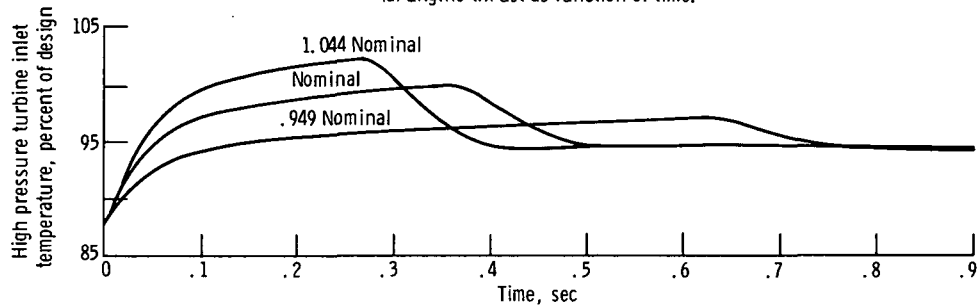
To evaluate the fuel control system proposed for the integral lift-fan engine (fig. 4), accelerations from the takeoff condition to the design thrust condition were run for both standard and hot days. It was decided that, for the range of rotor speeds involved, the acceleration schedule  $\phi_{max}$  could be approximated by a constant. Since the hybrid simulation uses total pressures, the computed values of  $\phi_{max}$  are approximately 4.3 percent lower than the actual values (fuel control uses static pressures) at the design point.

Effect of acceleration schedule. - Figure 7 shows the effect of changing the acceleration schedule  $\phi_{max}$  on the responses of thrust and turbine inlet temperature to a step change in throttle position. Standard-day conditions were assumed. The figure also shows the tradeoff between the reduced time constant  $\tau$  (time to achieve 63 percent  $\Delta F$ ) and the increased peak turbine inlet temperature  $T_4$ . The nominal value of  $\phi_{max}$  results in a time constant of 0.285 second with a peak turbine inlet temperature equal to 99.3 percent of the design value. The accepted response goal for a VTOL propulsion system is  $\tau \leq 0.20$  second (ref. 9). Figure 7(b) shows that turbine inlet temperature increases until the fuel control switches to closed-loop control of fan speed. The duration of turbine overtemperatures might prove to be as important a factor as peak temperatures. The tolerance of the integral engine to temperature excursions above the design value of  $T_4$  is undefined. The delay in achieving the final thrust value (see fig. 7(a)) is characteristic of the fuel control design and might be reduced by adding proportional action to the controller. This delay does not significantly degrade the overall performance of the engine.

Figure 8 shows the effect of  $\phi_{max}$  on the thrust and turbine inlet temperature responses, respectively, for the hot-day condition. Figure 8(a) indicates that a value of  $\phi_{max} = 1.044 \phi_{max, nom}$  is required to match the standard-day time constant of 0.285 second. The implementation of an ambient temperature-sensitive acceleration schedule might take the form shown in figure 4; that is, a temperature correction factor



(a) Engine thrust as function of time.



(b) High-pressure turbine inlet temperature as function of time.

Figure 7. - Effect of acceleration schedule  $\phi_{max}$  on engine response. Accelerations from takeoff to design thrust; standard-day, sea level static conditions; fuel control gains nominal.

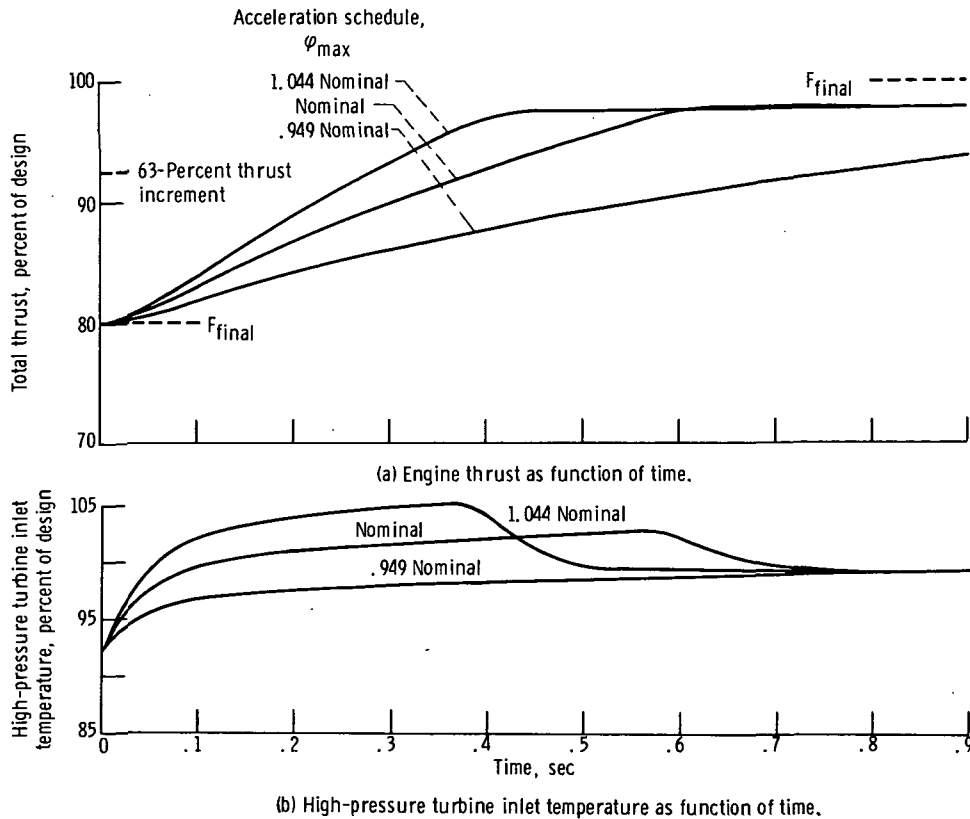


Figure 8. - Effect of acceleration schedule  $\varphi_{max}$  on engine response. Accelerations from takeoff to de-design thrust; hot-day, sea level static conditions; fuel control gains nominal.

T2C would be computed from the measured fan speed and used to modify the acceleration schedule  $\varphi_{max}(N_c)$ . Figure 8(b) shows a peak turbine inlet temperature equal to 1.051 times the design value resulting from the increased ambient temperature and acceleration limit.

To evaluate the sensitivity of the engine response to changes in the fuel control gains, standard-day accelerations from the takeoff condition to the design thrust condition were run. The nominal value of  $\varphi_{max}$  was used for these runs.

Effect of valve actuator gain. - The valve actuator gain  $K_V$  (see fig. 4) was varied from 0.2 to 4.0 times the nominal value. This gain affects both the initial phase of the acceleration (closed loop on valve position) and the latter phase (closed loop on fan speed). Figures 9(a) and (b) show the resulting standard-day responses of thrust and turbine inlet temperature, respectively. The lowest gain results in a sluggish response ( $\tau = 0.52$  second) with little overshoot in temperature. The highest gain resulted in a reduction in the time constant to  $\tau = 0.235$  second at the cost of slightly increased peak temperature (1.007 times design value) and a more oscillatory response.

Effect of valve rate feedback gain. - To increase the damping of the fuel control sys-

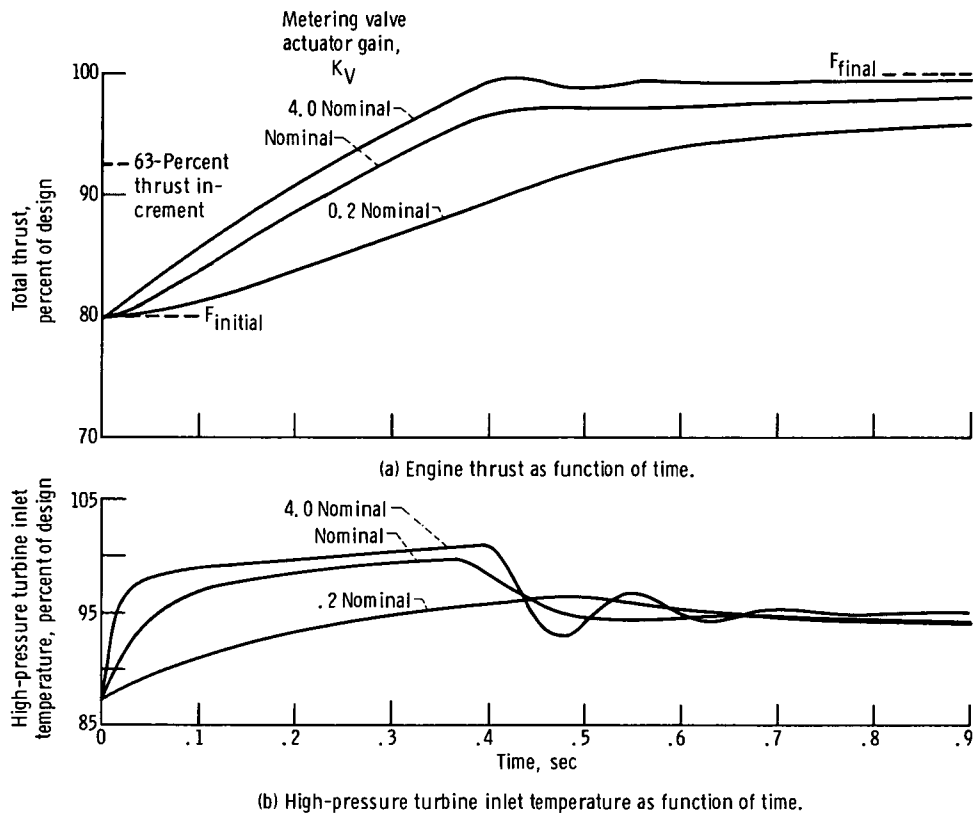


Figure 9. - Effect of fuel valve actuator gain  $K_V$  on engine response. Accelerations from takeoff to design thrust; standard-day, sea level static conditions; acceleration schedule,  $\phi_{max}$  = nominal; all other fuel control gains nominal.

tem, the rate feedback transfer function  $K_{AV}/(\tau_1 s + 1)$  is used to feed back the valve rate to the controller. To evaluate its effect on the engine response, the gain  $K_{AV}$  was varied from 0.1 to 2.0 times the nominal value for the standard-day accelerations. Figures 10(a) and (b) show the thrust and temperature responses for this case. They also show that the rate feedback only affects the closed-loop response after the fuel control switches from the acceleration schedule to the closed-loop control of fan speed. Decreasing  $K_{AV}$  results in slightly increased peak turbine inlet temperature while delaying the switch to fan speed control. As expected, decreased  $K_{AV}$  also results in a more oscillatory response. The nominal value results in a satisfactory response although  $K_{AV}$  might be decreased to hasten the achievement of maximum thrust at the cost of decreased damping.

Effect of temperature limiting. - Figures 8(a) and (b) indicate that significant turbine overtemperatures result when fast, hot-day accelerations to maximum thrust are run. Most turbojet and turbofan engines incorporate overtemperature limits in their control systems. To evaluate the response degradation associated with temperature limiting, the circuit shown in figure 11 was added to the fuel control system (see fig. 4). MIN circuit

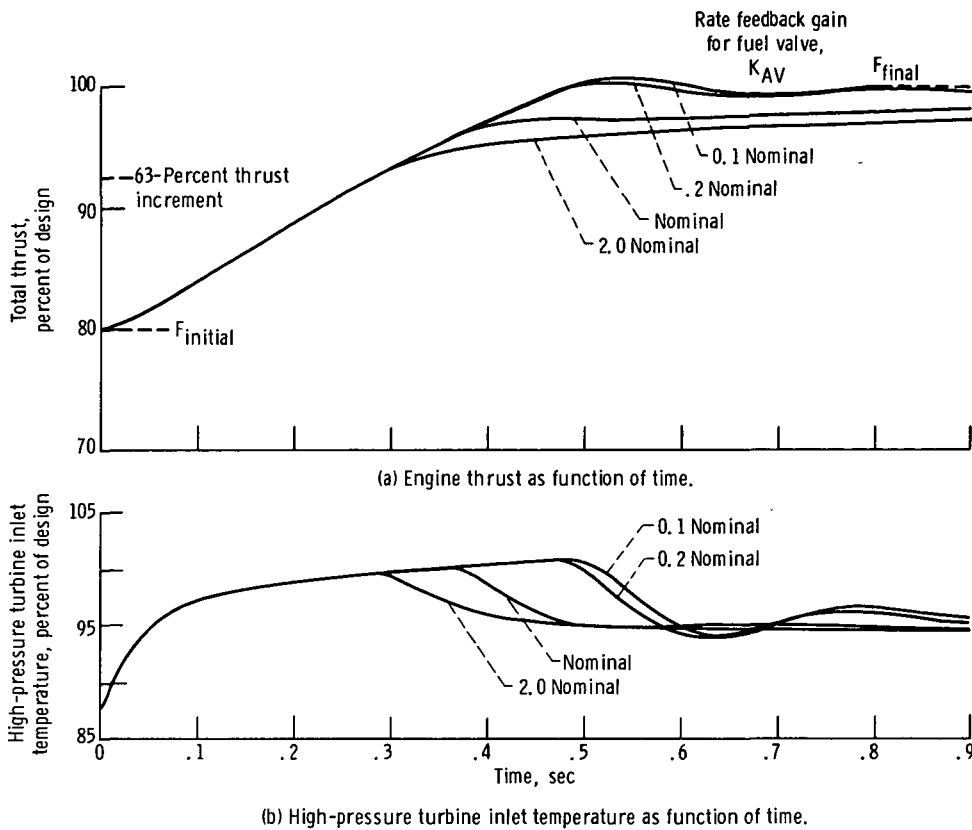


Figure 10. - Effect of fuel valve rate feedback gain  $K_{AV}$  on engine response. Accelerations from take-off to design thrust; standard-day, sea level static conditions; acceleration schedule,  $\varphi_{max}$  = nominal; all other fuel control gains nominal.

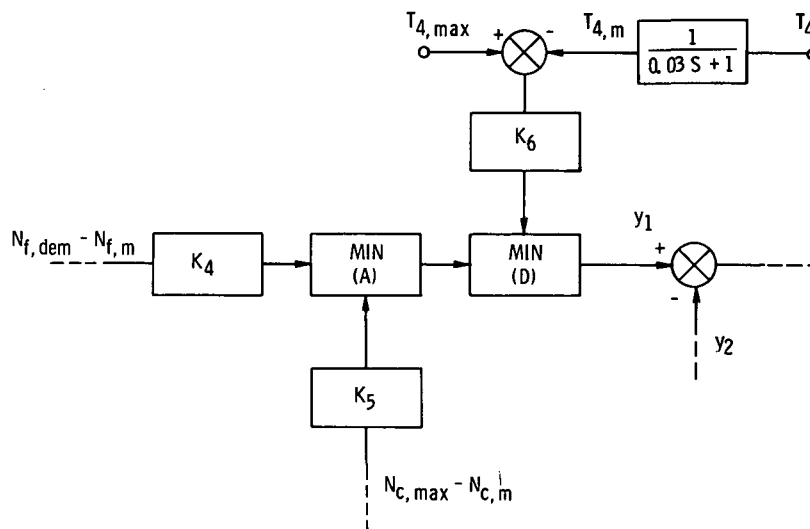


Figure 11. - Block diagram of temperature override in fuel control.

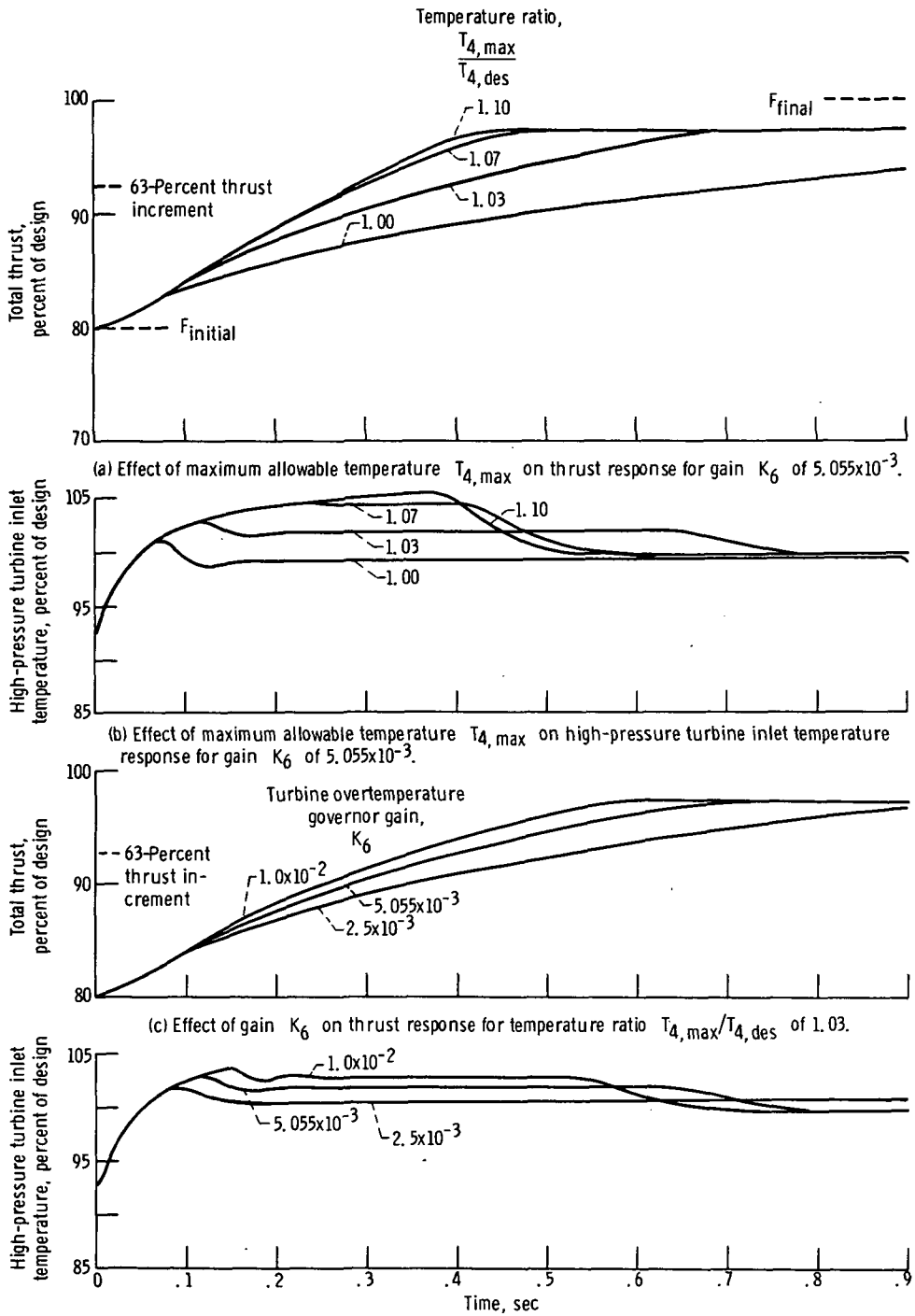


Figure 12. - Effect of temperature  $T_4$  limit on engine response. Accelerations from takeoff to design thrust; hot-day, sea level static conditions; acceleration schedule,  $\varphi_{\max} = 1.044$  nominal; fuel control gains nominal.

(D) was used with a gain  $K_6$  controlling the switch to closed-loop control of the inlet temperature  $T_4$  if the maximum allowable temperature  $T_{4,max}$  is approached. Figures 12(a) and (b) show the effect of the temperature limit on the hot-day responses of thrust and turbine inlet temperature, respectively. The acceleration schedule  $\phi_{max}$  was equal to 1.044 times the standard-day value for these runs. The gain  $K_6$  was set to  $5.055 \times 10^{-3}$  for the accelerations shown in figures 12(a) and (b). With the maximum allowable temperature  $T_{4,max}$  set to 1.10 times the design point value, the engine responses correspond to those obtained with no temperature limiting (see fig. 8). As  $T_{4,max}$  approaches the design point value, however, the thrust response becomes more sluggish. A value of  $T_{4,max}$  equal to  $1.03 T_{4,des}$  resulted in a 0.4-second time constant with the greater portion of the acceleration controlled by  $T_{4,max}$ . With  $T_{4,max}$  equal to  $T_{4,des}$ , the time constant increased to 0.735 second. Figures 12(c) and (d) show the effect of the gain  $K_6$  on the thrust and turbine temperature, respectively. Temperature  $T_{4,max}$  was set to  $1.03 T_{4,des}$  for these runs. Since increasing  $K_6$  delays the switch to temperature control (in addition to increasing the control gain), some reduction in the time constant is observed. With  $K_6$  equal to  $1.0 \times 10^{-2}$  the time constant was 0.34 second and the peak temperature was very nearly equal to the specified maximum.

While the fuel control gains were not optimized for this portion of the study, it is apparent that significant increases in the engine time constant can result from temperature limiting. The need for such limiting will be based on the tolerance of the turbines to the peak temperatures associated with rapid accelerations.

Effect of deceleration schedule. - Having determined the acceleration characteristics of the integral engine and fuel control, a study was undertaken to determine the mirror-imaginess of the engine's thrust responses.

While the engine manufacturer had assumed a deceleration schedule  $\phi_{min}$  equal to one-half the acceleration schedule  $\phi_{max}$ , the significance of this assumption was unknown. For comparison with available acceleration data, decelerations were run from the takeoff condition ( $0.8 F_{des}$ ) to the 60-percent thrust condition. Standard-day conditions were assumed with  $\phi_{max}$  equal to the nominal value and  $\phi_{min}/\phi_{max}$  varied from 0.5 to 0.7. Figure 13 shows the resultant thrust responses. A ratio of 0.65 results in the desired mirror-image characteristic. Similar decelerations were run for the hot-day condition with  $\phi_{max}$  equal to 1.044 times the nominal value. Figure 14 shows the resultant thrust responses. The ratio of 0.65 proved satisfactory for the hot-day condition, also. Figure 15 illustrates the effect of  $\phi_{min}/\phi_{max}$  on the deceleration time constant for both standard-day and hot-day conditions.

Effect of thrust level and thrust increment. - The response time of the integral engine is a function not only of the fuel control parameters but also of the thrust level and thrust increment. Standard-day accelerations from initial thrusts, ranging from the 45-percent level to the takeoff thrust (80 percent), were run using the nominal fuel control.

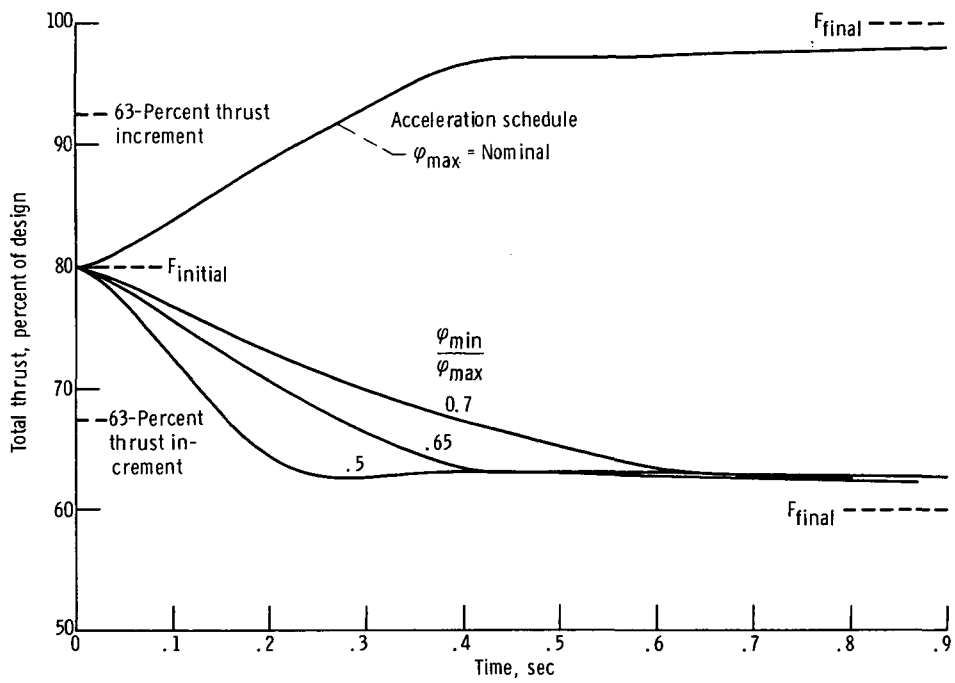


Figure 13. - Effect of deceleration schedule  $\varphi_{min}$  on engine thrust response. Decelerations from takeoff to 60-percent thrust; standard-day, sea level static conditions; fuel control gains nominal.

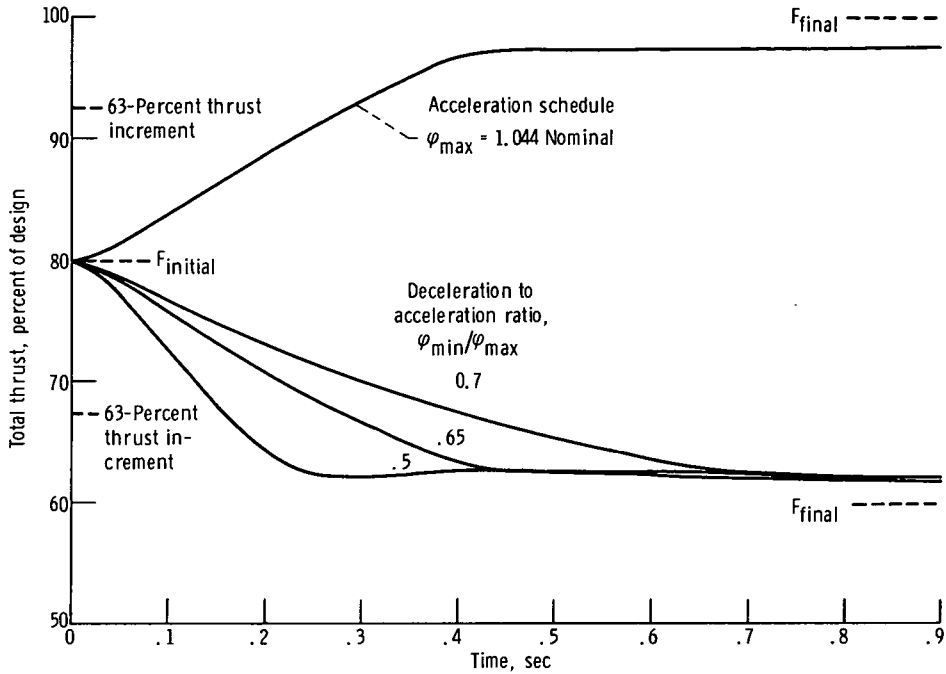


Figure 14. - Effect of deceleration schedule  $\varphi_{\min}$  on engine thrust response. Decelerations from takeoff to 60-percent thrust; hot-day, sea level static conditions; fuel control gains nominal.

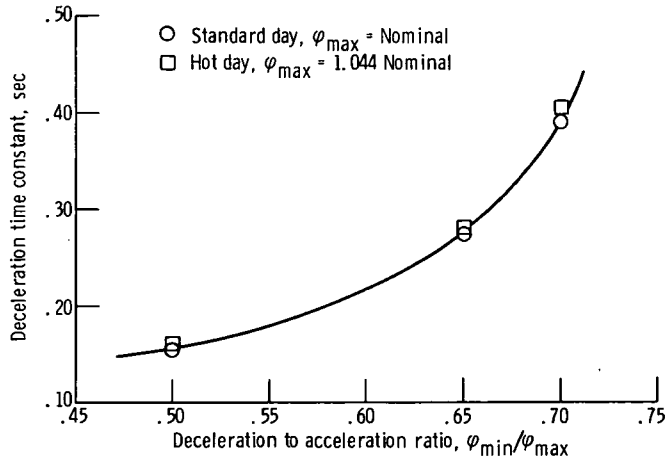
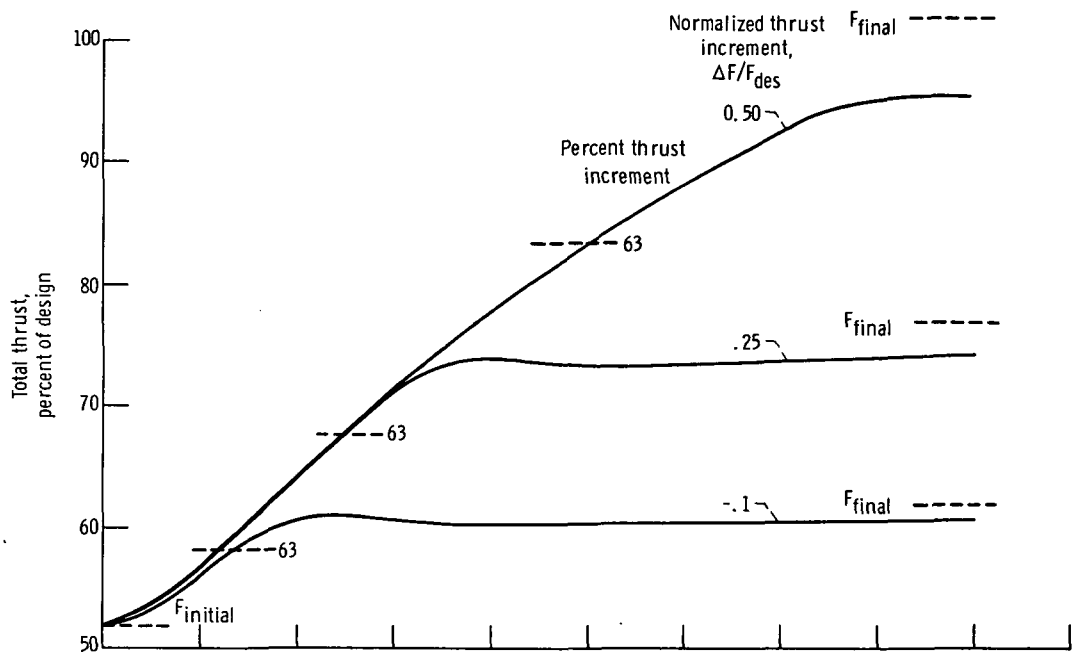
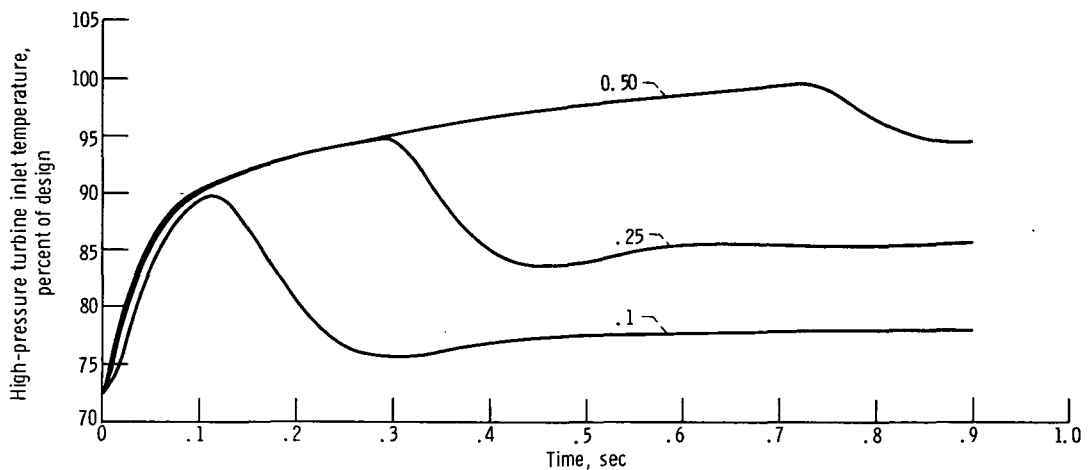


Figure 15. - Effect of deceleration schedule  $\varphi_{\min}$  on engine time constant. Decelerations from takeoff to 60-percent thrust; fuel control gains nominal; sea level static conditions.



(a) Engine thrust as function of time.



(b) High-pressure turbine inlet temperature as function of time.

Figure 16. - Effect of thrust increment on engine response. Accelerations from landing thrust; standard-day, sea level static conditions; acceleration schedule,  $\varphi_{\max}$  = nominal; fuel control gains nominal.

The assumption of  $\varphi_{\min}/\varphi_{\max} = 0.50$  was used to allow comparisons with contractor-generated data. Decelerations were also run from thrust levels ranging from the design thrust to 65-percent thrust. Figures 16(a) and (b) show the responses of thrust and turbine inlet temperature, respectively, for the accelerations from the landing condition (52-percent thrust). The time constants for all accelerations and decelerations are plotted in figure 17 as functions of the initial thrust level and the thrust increment  $\Delta F$ . Time constants as low as 0.095 second (for the 10-percent  $F_{\text{des}}$  deceleration from the design thrust) and as high as 0.53 second (for the 50-percent  $F_{\text{des}}$  acceleration from the 55-

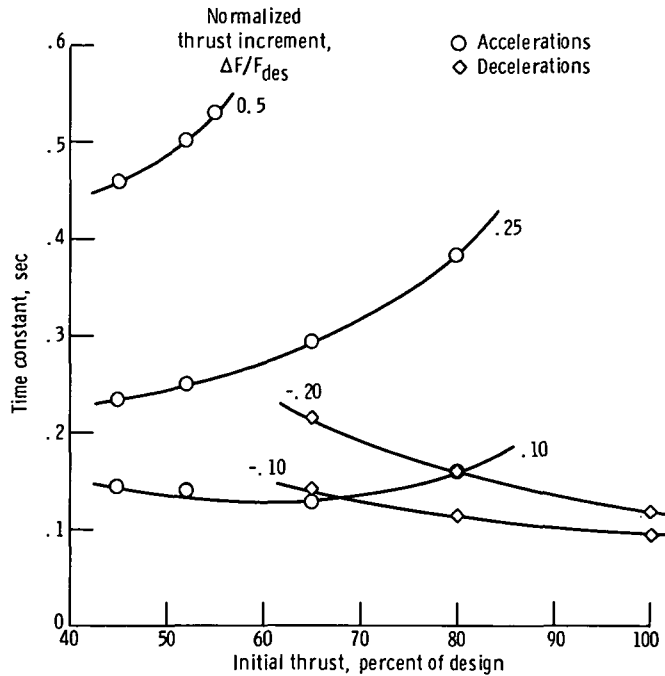
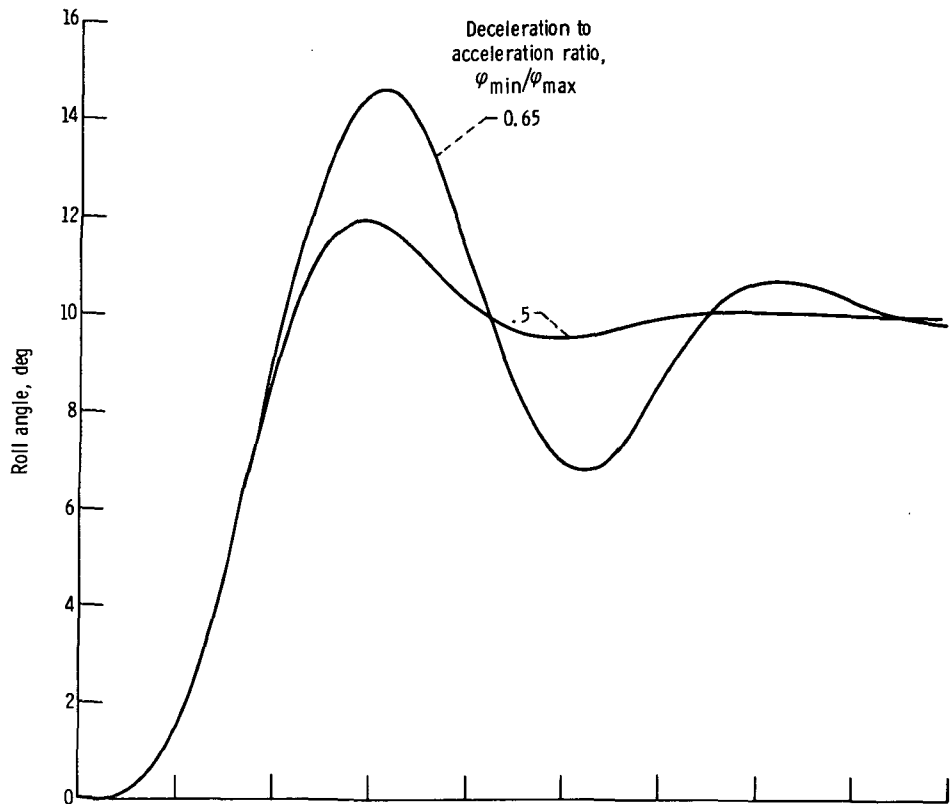


Figure 17. - Effect of initial thrust and thrust increment on engine time constant. Standard-day, sea level static conditions; acceleration schedule,  $\varphi_{\max}$  = nominal; deceleration schedule,  $\varphi_{\min}$  =  $0.5 \varphi_{\max}$ ; fuel control gains nominal.

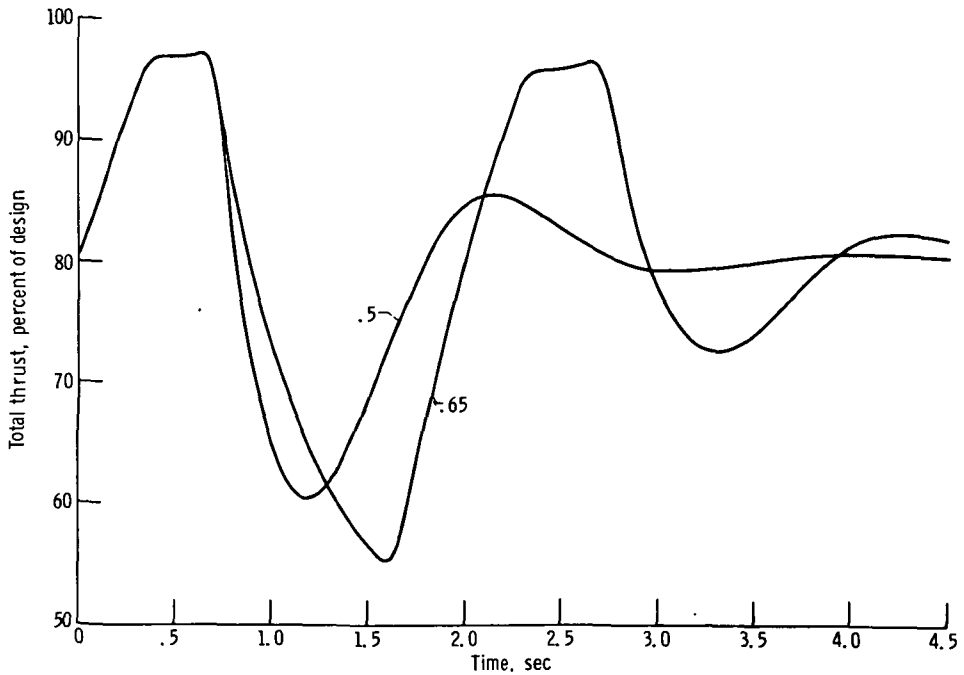
percent thrust level) were observed using the simulation. Figure 17 indicates that the desired response goal ( $\tau \leq 0.20$  sec) is achieved for thrust increments less than 10 percent of the design thrust. Most accelerations and decelerations during flight would involve thrust increments of this magnitude.

## Roll Control - Airplane Response

10° Roll maneuver. - To aid in ascertaining the response interactions of the integral engine fuel control with a VTOL airplane, the aircraft roll control (fig. 6) was added to the hybrid simulation. A standard-day hovering condition at takeoff thrust was assumed. To allow possible comparisons with contractor data, the ratio  $\varphi_{\min}/\varphi_{\max}$  was set to 0.5. With the engine operating at the takeoff condition (80-percent thrust), a 10° (0.1745 rad) roll angle demand was input to the roll control system. Figures 18(a) and (b) show the resulting responses of roll angle  $\theta$  and engine thrust, respectively. All controller gains were nominal with  $\varphi_{\max}$  equal to the nominal value. A peak roll angle of 11.9° (0.2077 rad) was observed with a roll angle of 8.9° (0.1553 rad) achieved in 1 second. A goal of reaching the demanded roll angle in 1 second with less than 10-percent overshoot is desirable for a VTOL airplane. Figure 18(a) indicates that this goal



(a) Roll angle as function of time.



(b) Engine thrust as function of time.

Figure 18. - Effect of deceleration schedule  $\varphi_{\min}$  on engine-airplane response to  $10^\circ$  roll angle demand. Hovering at takeoff thrust; standard-day, sea level static conditions;  $\varphi_{\max}$  = nominal; fuel control and roll control gains nominal.

might be achieved with some modification in the airplane and/or control system. Some modification to the roll control system might also be required to eliminate the 0.25-second deadtime observed in the roll angle response. Figure 19 shows strip-chart recordings of selected engine and roll control variables for the standard-day roll maneuver.

Effect of deceleration schedule. - The same roll maneuver was run with the value of  $\varphi_{\min}/\varphi_{\max} = 0.65$ . This value results in the assumed mirror-image thrust responses for accelerations and decelerations from the takeoff condition. Figures 18(a) and (b) show the effect of the increased  $\varphi_{\min}$  on the roll angle and thrust responses, respectively. The increased fuel flow results in a slower deceleration in response to the roll angle overshoot. A peak roll angle of  $14.6^\circ$  (0.2548 rad) results with a significant decrease in the system damping. Figures 18(a) and (b) indicate that the selection of control gains must account for any modifications made in the fuel control system.

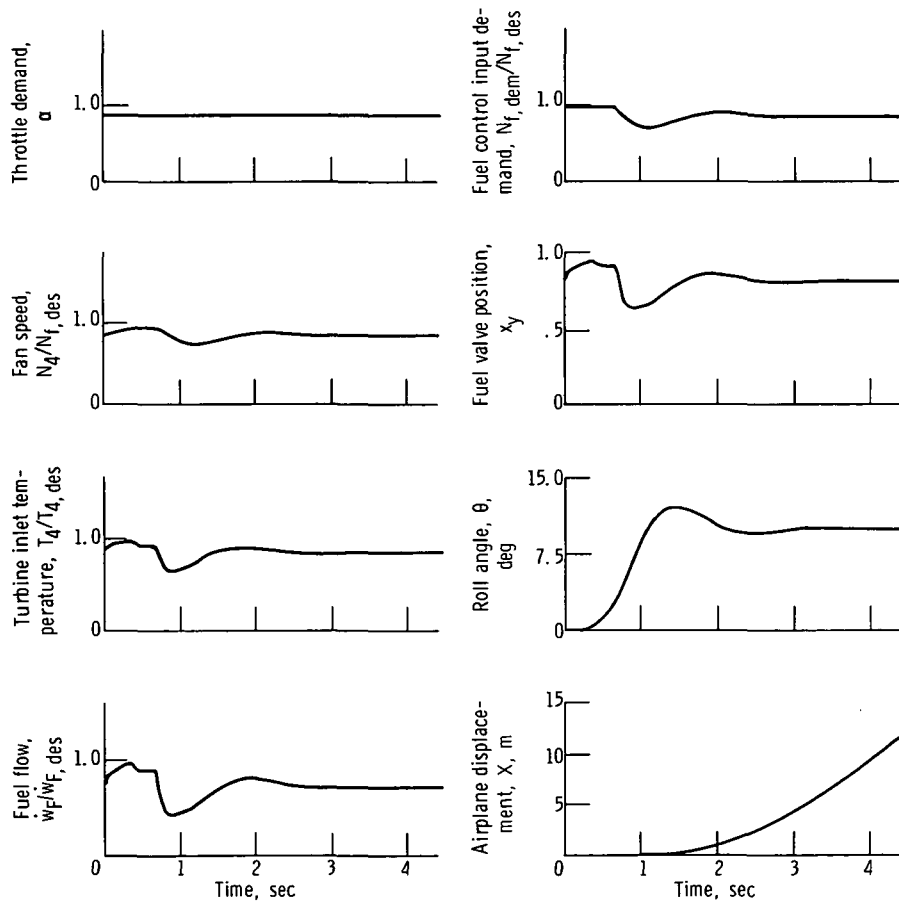


Figure 19. - Response of selected engine-airplane variables to  $10^\circ$  roll angle demand. Hovering at takeoff thrust; standard-day, sea level static conditions; acceleration schedule,  $\varphi_{\max}$  = nominal; deceleration schedule,  $\varphi_{\min} = 0.5 \varphi_{\max}$ ; fuel control and roll control gains nominal.

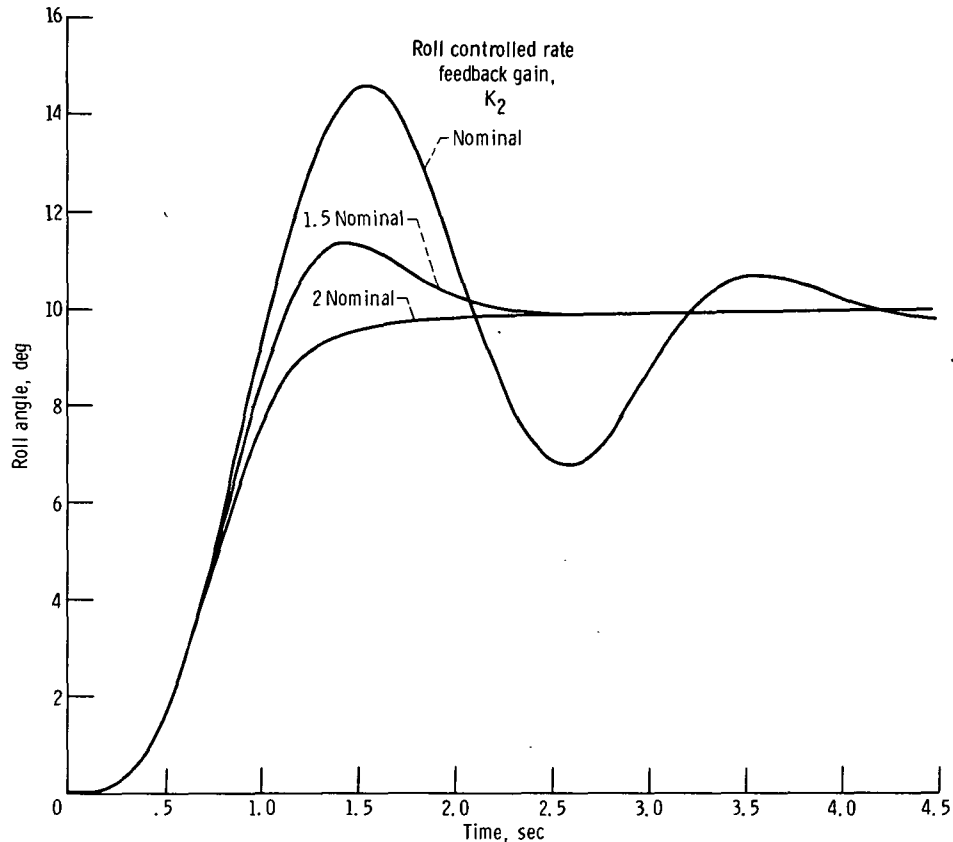


Figure 20. - Effect of roll rate feedback gain  $K_2$  on airplane response to  $10^\circ$  roll angle demand. Hovering at takeoff thrust; standard-day, sea level static conditions; acceleration schedule,  $\varphi_{\max}$  = nominal; deceleration schedule,  $\varphi_{\min} = 0.65 \varphi_{\max}$ ; all other fuel control and roll control gains nominal.

Effect of roll rate feedback gain. - To increase the closed-loop system damping with the desired  $\varphi_{\min}/\varphi_{\max} = 0.65$ , the roll rate feedback gain  $K_2$  was varied from the nominal value to twice the nominal value. Figure 20 shows the resulting roll angle responses for the standard-day,  $10^\circ$  (0.1745 rad) roll maneuver. A 50-percent increase in the nominal roll rate feedback gain results in a peak roll angle of  $11.3^\circ$  (0.1972 rad) with a roll angle of  $8.4^\circ$  (0.1466 rad), achieved in 1 second.

Effect of roll angle demand. - As in the case of throttle demands, the response characteristics of the roll control system are affected by the size of the input demand. Figure 21 shows the response of roll angle to roll angle demands ranging from  $3.75^\circ$  to  $10^\circ$  (0.0654 to 0.1745 rad) for standard-day, takeoff conditions. The increased roll rate feedback gain was used for these runs. The effective damping of the closed-loop system decreases as the roll angle demand increases. There is virtually no overshoot in the roll angle for input demands less than  $5^\circ$  (0.0873 rad). The roll angle, achieved in 1 second, varied from 84 percent ( $10^\circ$  demand) to 92 percent (less than  $5^\circ$  demand) of the demanded roll angle. These results are encouraging since a typical hovering maneuver

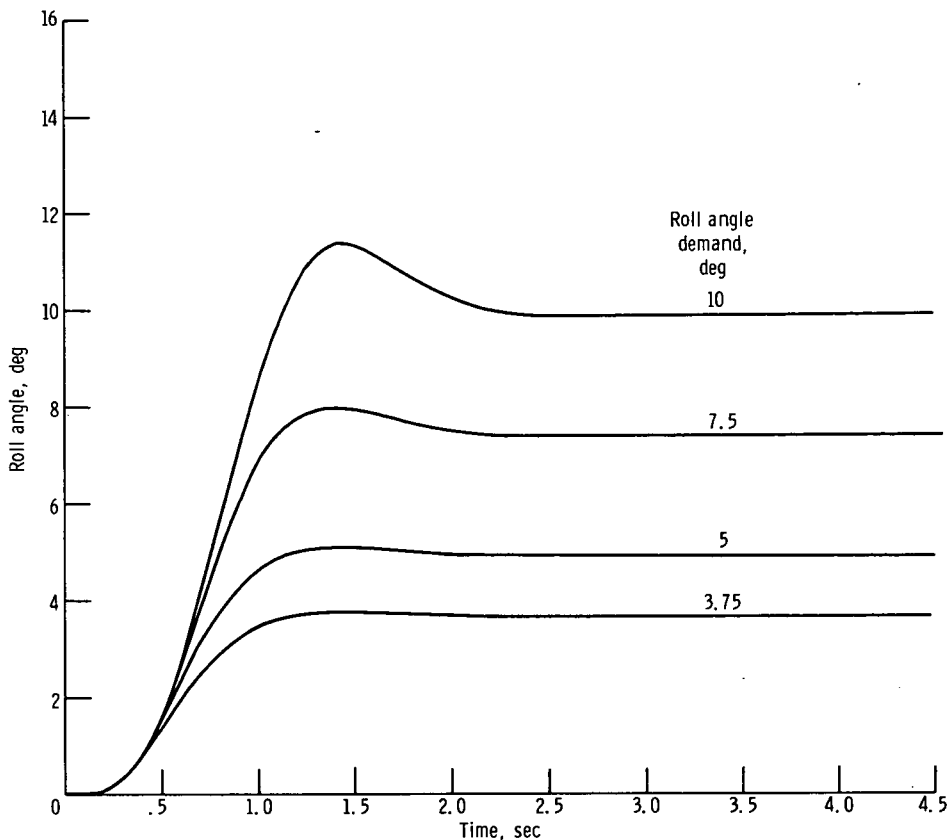
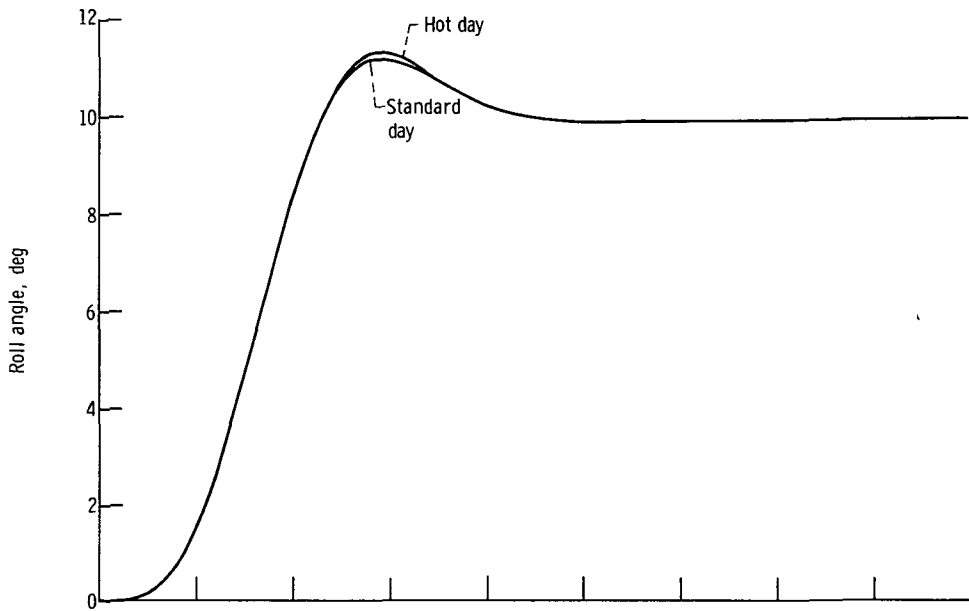


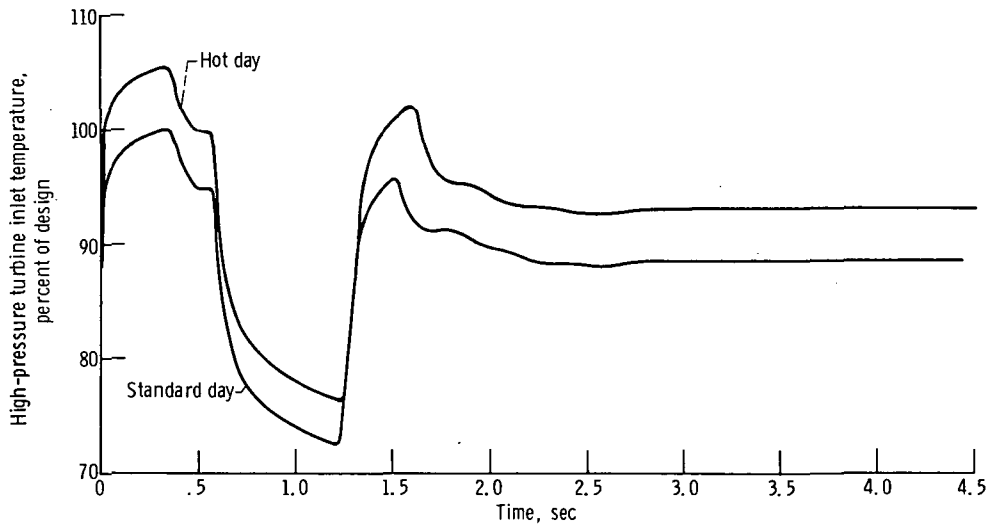
Figure 21. - Effect of roll angle demand on airplane response. Hovering at takeoff thrust; standard-day, sea level static conditions; acceleration schedule,  $\varphi_{\max}$  = nominal; deceleration schedule,  $\varphi_{\min}$  =  $0.65 \varphi_{\max}$ ; gain,  $K_2$  = 1.5 nominal; all other fuel control and roll control gains nominal.

might involve roll angle demands of  $\pm 3^\circ$  ( $\pm 0.0524$  rad).

Effect of ambient temperature. - As mentioned previously, a determining factor in the achievement of fast response will be the tolerance of the integral engine to the potential turbine overtemperatures associated with hot-day accelerations of the engine. Since no contractor data for hot-day operation were available, the  $10^\circ$  ( $0.1745$  rad) roll maneuver was simulated at the hot-day takeoff condition with the increased roll rate feedback gain. The increased ambient temperature was reflected in (1) increased throttle demand  $N_{f, \text{dem}, \alpha}$  to achieve the takeoff thrust (80-percent thrust), (2) increased roll error demand  $N_{f, \text{dem}, \theta}$ , (3) increased limits on the fuel control input demand  $N_{f, \text{dem}}$ , and (4) increased acceleration schedule  $\varphi_{\max}$ . Figures 22(a) and (b) show a comparison of the standard-day and hot-day responses of roll angle and turbine inlet temperature, respectively. Figure 22(a) shows that virtually identical responses of  $\theta$  are achieved by the temperature compensations previously described. Figure 22(b) shows the expected increase in turbine temperature due to the hot-day condition. In addition to the peak tem-



(a) Roll angle as function of time.



(b) High-pressure turbine inlet temperature as function of time.

Figure 22. - Effect of ambient temperature on engine-airplane response to  $10^0$  roll angle demand. Hovering at takeoff thrust; sea level static conditions; deceleration schedule,  $\varphi_{\min} = 0.65 \varphi_{\max}$ ; gain,  $K_2 = 1.5$  nominal; all other fuel control and roll control gains nominal.

perature (1.054 times the design point temperature), the rapid changes in turbine temperature associated with the  $10^0$  roll maneuver might have an undesirable effect on the engine.

## SUMMARY OF RESULTS

An integral lift-fan engine, proposed for use in a VTOL airplane, was simulated on the hybrid computer using a general engine simulation program. A fuel control system and a VTOL airplane roll control system were added to the engine simulation. Sea level static conditions were assumed. The results of the hybrid computer studies indicated the following:

1. The nominal acceleration schedule results in a 0.285-second time constant for a standard-day takeoff to design thrust acceleration. The desired response goal of  $\tau \leq 0.20$  second was achieved for thrust increments less than 10 percent of the design thrust.
2. Increasing the standard-day acceleration schedule 4.4 percent results in a 0.285-second time constant for the hot-day takeoff to design thrust acceleration; the increased ambient temperature and fuel flow results in a peak turbine inlet temperature 5.4 percent higher than the design point value.
3. Although not optimized, the nominal fuel control gains result in satisfactory thrust response characteristics. An increased fuel valve actuator gain resulted in slight reductions in the time constant at the cost of increased peak turbine temperature.
4. The use of a temperature limit in the fuel control can seriously degrade the hot-day acceleration to design thrust. Limiting the turbine inlet temperature to the design point value increased the time constant from 0.285 to 0.735 second.
5. The use of the contractor's assumed relationship between the deceleration and acceleration schedules ( $\varphi_{\min} = 0.5 \varphi_{\max}$ ) does not result in the desired mirror-image thrust responses. A ratio of  $\varphi_{\min}/\varphi_{\max} = 0.65$  proved to be satisfactory for both standard-day and hot-day conditions.
6. The use of  $\varphi_{\min}/\varphi_{\max} = 0.65$  results in an unsatisfactory roll angle response with the nominal roll control gains. For a standard-day  $10^0$  roll demand, a 46-percent overshoot in roll angle was observed indicating significant interaction between the fuel control and roll control systems. A 50-percent increase in the nominal roll rate feedback gain with  $\varphi_{\min} = 0.65 \varphi_{\max}$  resulted in a satisfactory roll angle response. For a  $10^0$  roll angle demand, a 13-percent overshoot was observed with 84 percent of the demand achieved in 1 second. For roll demands less than  $5^0$ , no overshoot was observed with 92 percent of the demand achieved in 1 second.

7. The use of temperature-sensitive throttle gain, roll control forward gain, acceleration schedule, and fuel control input limits results in virtually identical roll-angle responses for both standard-day and hot-day conditions.

The results of this study indicate that the integral engine concept lends promise of achieving the response goals of a VTOL propulsion system. The determining factor in the achievement of the desired 0.20-second time constant for large thrust increments will be the tolerance of the turbines to overtemperatures during accelerations to design thrust. Once this tolerance is known, acceleration schedules, controller gains, etc. can be optimized to accomplish the necessary reduction in response time.

Lewis Research Center,  
National Aeronautics and Space Administration,  
Cleveland, Ohio, September 19, 1972,  
764-72.

# APPENDIX A

## SYMBOLS

A	effective cross-sectional area, $\text{cm}^2$ ( $\text{in.}^2$ )
$c_p$	specific heat at constant pressure, $\text{J/kg-K}$ ( $\text{Btu/lbm-}^\circ\text{R}$ )
$c_v$	specific heat at constant volume, $\text{J/kg-K}$ ( $\text{Btu/lbm-}^\circ\text{R}$ )
cnp	compressor speed parameter
ctr	compressor ideal temperature rise parameter
d	slope of supercharger performance map, $\text{N/cm}^2$ ( $\text{lbf/in.}^2$ )
dt	differential time, sec
e	intercept of supercharger performance map, $\text{N/cm}^2$ ( $\text{lbf/in.}^2$ )
F	thrust, N (lbf)
$\mathcal{F}_i$	functional relationship
$\Delta F$	thrust increment, N (lbf)
f/a	fuel-air ratio
fcnp	general fan or compressor map speed parameter
fnp	fan speed parameter
fpc	compressor map flow parameter, $\text{kg/sec}$ ( $\text{lbm/sec}$ )
fpf	fan map flow parameter, $\text{kg/sec}$ ( $\text{lbm/sec}$ )
fpfe	general fan or compressor map flow parameter, $\text{kg/sec}$ ( $\text{lbm/sec}$ )
fpt	high-pressure turbine map flow parameter, $\text{kg-K-cm}^2/\text{N-rpm-sec}$ ( $\text{lbm-}^\circ\text{R-in.}^2/\text{lbf-rpm-sec}$ )
fpt1	high-pressure turbine map flow parameter, $\text{kg-K-cm}^2/\text{N-fpm-sec}$ ( $\text{lbm-}^\circ\text{R-in.}^2/\text{lbf-rpm-sec}$ )
fpt2	low-pressure turbine map flow parameter, $\text{kg-K-cm}^2/\text{N-rpm-sec}$ ( $\text{lbm-}^\circ\text{R-in.}^2/\text{lbf-rpm-sec}$ )
ftr	fan ideal temperature rise parameter
$g_c$	gravitational conversion factor, $100 \text{ cm-kg/N-sec}^2$ ( $386.3 \text{ lbm-in./lbf-sec}^2$ )
HVF	heating value of fuel, $\text{J/kg}$ ( $\text{Btu/lbm}$ )
$\Delta h$	turbine enthalpy drop, $\text{J/kg}$ ( $\text{Btu/lbm}$ )

hpt	general turbine map enthalpy drop parameter, $J/kg-K^{1/2}$ -rpm (Btu/lbm- $^{\circ}R^{1/2}$ -rpm)
hpt1	high-pressure turbine map enthalpy drop parameter, $J/kg-K^{1/2}$ -rpm (Btu/lbm- $^{\circ}R^{1/2}$ -rpm)
hpt2	low-pressure turbine map enthalpy drop parameter, $J/kg-K^{1/2}$ -rpm (Btu/lbm- $^{\circ}R^{1/2}$ -rpm)
I	polar moment of inertia, N-cm-sec <sup>2</sup> (in. -lbf-sec <sup>2</sup> )
J	work conversion factor, 100 N-cm/J (9339.6 in. -lbf/Btu)
K <sub>AC</sub>	valve position controller gain
K <sub>AV</sub>	rate feedback gain for fuel valve
K <sub>mv</sub>	metering valve flow coefficient
K <sub>V</sub>	metering valve actuator gain
K <sub>X</sub>	distance conversion factor, 0.0833 ft/in. (1.0)
K <sub>1</sub>	roll controller forward gain, rpm/deg
K <sub>2</sub>	roll controller rate feedback gain, rpm-sec/deg
K <sub>3</sub>	speed controller forward gain
K <sub>4</sub>	fan speed controller gain
K <sub>5</sub>	compressor overspeed governor gain
K <sub>6</sub>	turbine overtemperature governor gain
K <sub>θ</sub>	angle conversion factor, 57.32 <sup>o</sup>
L	torque, N-cm (in. -lbf)
ΔL	differential torque, N-cm (lbf-in.)
l	length, cm (in.)
MM	number of flows fed by control volume
N	rotational speed, rpm
NN	number of flows feeding control volume
n <sub>E</sub>	number of engines
P	total pressure, N/cm <sup>2</sup> (psia)
P <sub>s</sub>	static pressure, N/cm <sup>2</sup> (psia)
pr	pressure ratio

prc	compressor map pressure ratio
prf	fan map pressure ratio
prt1	high-pressure turbine map pressure ratio
prt2	low-pressure turbine map pressure ratio
R	gas constant, N-cm/kg-K (in. -lbf/lbm- <sup>o</sup> R)
$\mathcal{R}$	duct pressure loss coefficient, N-sec <sup>2</sup> /kg <sup>2</sup> -cm <sup>2</sup> (lbf-sec <sup>2</sup> /lbm <sup>2</sup> -in. <sup>2</sup> )
r <sub>AP</sub>	roll moment arm, in. (cm)
s	Laplace operator, sec <sup>-1</sup>
T	total temperature, K ( <sup>o</sup> R)
T2C	temperature-sensitive corrector factor on acceleration schedule
t	time, sec
tnp	general turbine map speed parameter, rpm/K <sup>1/2</sup> (rpm/ <sup>o</sup> R <sup>1/2</sup> )
t1np	high-pressure turbine map speed parameter, rpm/K <sup>1/2</sup> (rpm/ <sup>o</sup> R <sup>1/2</sup> )
t2np	low-pressure turbine map speed parameter, rpm/K <sup>1/2</sup> (rpm/ <sup>o</sup> R <sup>1/2</sup> )
tr	general fan or compressor ideal temperature rise parameter
trsc	supercharger ideal temperature rise parameter
V	volume, cm <sup>3</sup> (in. <sup>3</sup> )
W	mass, kg (lbm)
$\dot{w}$	mass flow, kg/sec (lbm/sec)
X	aircraft lateral displacement, cm (ft)
x <sub>v</sub>	valve displacement, cm (in.)
y <sub>i</sub>	general fuel control variable (appropriate units)
$\alpha$	relative throttle position
$\beta$	temperature interpolation constant
$\gamma$	specific heat ratio
$\eta$	efficiency
$\theta$	roll angle, deg (rad)
$\tau$	time constant, sec
$\tau_1$	fuel valve rate feedback time constant, sec
$\varphi$	fuel flow parameter, kg-cm <sup>2</sup> /N-sec (lbm/sec/psi)

**Subscripts:**

<b>A</b>	<b>air</b>
<b>AP</b>	<b>airplane</b>
<b>a</b>	<b>ambient</b>
<b>accel</b>	<b>acceleration</b>
<b>b</b>	<b>burner</b>
<b>bl1</b>	<b>high-pressure turbine cooling bleed</b>
<b>bl2</b>	<b>low-pressure turbine cooling bleed</b>
<b>c</b>	<b>compressor</b>
<b>cd</b>	<b>core duct</b>
<b>cr</b>	<b>critical</b>
<b>decel</b>	<b>deceleration</b>
<b>dem</b>	<b>demand</b>
<b>des</b>	<b>design</b>
<b>F</b>	<b>fuel</b>
<b>f</b>	<b>fan</b>
<b>i</b>	<b>initial condition</b>
<b>m</b>	<b>measured</b>
<b>max</b>	<b>maximum</b>
<b>min</b>	<b>minimum</b>
<b>nom</b>	<b>nominal</b>
<b>ovb</b>	<b>overboard bleed</b>
<b>SC</b>	<b>supercharger</b>
<b>std</b>	<b>standard day</b>
<b>t1</b>	<b>high-pressure turbine</b>
<b>t2</b>	<b>low-pressure turbine</b>
<b>tot</b>	<b>total engine</b>
<b><math>\alpha</math></b>	<b>throttle demand</b>
<b><math>\theta</math></b>	<b>roll demand</b>
<b>2</b>	<b>fan inlet</b>

- 2.1 supercharger-compressor intercomponent volume
- 2.5 fan duct volume
- 2.8 fan nozzle volume
- 3 compressor-combustor intercomponent volume
- 4 combustor volume
- 5 high-pressure turbine/low-pressure turbine intercomponent volume
- 5.1 one-half of core duct volume (upstream)
- 6 one-half of core duct volume (downstream)
- 8 core nozzle throat
- 70 70-percent maximum thrust
- 100 100-percent maximum thrust

Superscripts:

- average
- ' inlet of control volume
- time derivative

## APPENDIX B

### SUMMARY OF EQUATIONS

Engine:

$$\text{prf} = \frac{P_{2.5}}{P_2} \quad (\text{B1})$$

$$\text{fnp} = \frac{N_f/N_{f, \text{des}}}{\sqrt{T_2/T_{2, \text{des}}}} \quad (\text{B2})$$

$$\text{fpf} = \mathcal{F}_{1, f}(\text{prf}, \text{fnp}) \quad (\text{B3})$$

$$\dot{w}_{2.5} = \frac{\text{fpf}(P_2/P_{\text{std}})}{\sqrt{T_2/T_{\text{std}}}} \quad (\text{B4})$$

$$\eta_f = \mathcal{F}_{2, f}(\text{prf}, \text{fnp}) \quad (\text{B5})$$

$$\gamma_f = \mathcal{F}_5(\bar{T}_f, 0) \quad (\text{B6})$$

$$c_{p_f} = \mathcal{F}_6(\bar{T}_f, 0) \quad (\text{B7})$$

$$\bar{T}_f = \beta_f T_2 + (1 - \beta_f) T_{2.5} \quad (\text{B8})$$

$$\text{ftr} = \left( \frac{P_{2.5}}{P_2} \right)^{\gamma_f - 1/\gamma_f} - 1.0 \quad (\text{B9})$$

$$T'_{2.5} = \left[ \left( \frac{\text{ftr}}{\eta_f} \right) + 1.0 \right] T_2 \quad (\text{B10})$$

$$L_f = \frac{30J}{\pi} \frac{c_{p_f} (T'_{2.5} - T_2) \dot{w}_{2.5}}{N_f} \quad (\text{B11})$$

$$c'_{p_{2.5}} = \mathcal{F}_6(T'_{2.5}, 0) \quad (\text{B12})$$

$$P_{2.1} = d(\text{fnp}) + e \quad (\text{B13})$$

$$\text{trsc} = \left( \frac{P_{2.1}}{P_2} \right)^{0.286} - 1.0 \quad (\text{B14})$$

$$T_{2.1} = \left[ \frac{\text{trsc}}{\eta_{\text{SC}}} + 1.0 \right] T_2 \quad (\text{B15})$$

$$L_{\text{SC}} = \frac{\frac{30J}{\pi} c_{p_{\text{SC}}} (T_{2.1} - T_2) \dot{w}_3}{N_f} \quad (\text{B16})$$

$$\text{prc} = P_3/P_{2.1} \quad (\text{B17})$$

$$\text{cnp} = \frac{N_c/N_{c, \text{des}}}{\sqrt{T_{2.1}/T_{2.1, \text{des}}}} \quad (\text{B18})$$

$$\text{fpc} = \mathcal{F}_{1,c}(\text{prc}, \text{cnp}) \quad (\text{B19})$$

$$\dot{w}_3 = \frac{\text{fpc}(P_{2.1}/P_{\text{std}})}{\sqrt{T_{2.1}/T_{\text{std}}}} \quad (\text{B20})$$

$$\eta_c = \mathcal{F}_{2,c}(\text{prc}, \text{cnp}) \quad (\text{B21})$$

$$\gamma_c = \mathcal{F}_5(\bar{T}_c, 0) \quad (\text{B22})$$

$$c_{p_c} = \mathcal{F}_6(\bar{T}_c, 0) \quad (\text{B23})$$

$$\bar{T}_c = \beta_c T_{2.1} + (1 - \beta_c) T_3 \quad (\text{B24})$$

$$\text{ctr} = \left( \frac{P_3}{P_{2.1}} \right)^{\gamma_c - 1/\gamma_c} - 1.0 \quad (\text{B})$$

$$T_3' = \left[ \left( \frac{\text{ctr}}{\eta_c} \right) + 1.0 \right] T_{2.1} \quad (\text{B26})$$

$$L_c = \frac{\frac{30J}{\pi} c_{p_c} (T_3' - T_{2.1}) \dot{w}_3}{N_c} \quad (\text{B27})$$

$$c_{p_3}' = \mathcal{F}_6(T_3', 0) \quad (\text{B28})$$

$$t_{1np} = \frac{N_c}{\sqrt{T_4}} \quad (\text{B29})$$

$$\text{prt1} = P_5/P_4 \quad (\text{B30})$$

$$\text{fpt1} = \mathcal{F}_{3,t1}(\text{prt1}, t_{1np}) \quad (\text{B31})$$

$$\dot{w}_5 = \frac{\text{fpt1} P_4' N_c}{T_4} \quad (\text{B32})$$

$$\text{hpt1} = \mathcal{F}_{4,t1}(\text{prt1}, t_{1np}) \quad (\text{B33})$$

$$\Delta h_{t1} = \frac{\text{hpt1} N_c \sqrt{T_4}}{1000} \quad (\text{B34})$$

$$c_{p_{t1}} = \mathcal{F}_6 \left[ \bar{T}_{t1}, \left( \frac{f}{a} \right)_4 \right] \quad (\text{B35})$$

$$\bar{T}_{t1} = \beta_{t1} T_4 + (1 - \beta_{t1}) T_5 \quad (\text{B36})$$

$$L_{t1} = \frac{\frac{30J}{\pi} \Delta h_{t1} \dot{w}_5}{N_c} \quad (\text{B37})$$

$$T'_5 = T_4 \left[ 1.0 - \frac{\Delta h_{t1}}{(c_{p_{t1}} T_4)} \right] \quad (\text{B38})$$

$$c'_{p_s} = \mathcal{F}_6 \left[ T'_{s'}, \left( \frac{f}{a} \right)_4 \right] \quad (\text{B39})$$

$$\left( \frac{f}{a} \right)_4 = \frac{\dot{w}_F}{\dot{w}_4} \quad (\text{B40})$$

$$t_{2np} = \frac{N_f}{\sqrt{T_5}} \quad (\text{B41})$$

$$prt2 = P_{5.1}/P_5 \quad (\text{B42})$$

$$fpt2 = \mathcal{F}_{3,t2}(prt2, t_{2np}) \quad (\text{B43})$$

$$\dot{w}_{5.1} = \frac{fpt2 P_5 N_f}{T_5} \quad (\text{B44})$$

$$hpt2 = \mathcal{F}_{4,t2}(prt2, t_{2np}) \quad (\text{B45})$$

$$\Delta h_{t2} = \frac{hpt2 N_f \sqrt{T_5}}{1000} \quad (\text{B46})$$

$$c_{p_{t2}} = \mathcal{F}_6 \left[ \bar{T}_{t2}, \left( \frac{f}{a} \right)_5 \right] \quad (\text{B47})$$

$$\bar{T}_{t2} = \beta_{t2} T_5 + (1 - \beta_{t2}) T_{5.1} \quad (\text{B48})$$

$$L_{t2} = \frac{\frac{30J}{\pi} \Delta h_{t2} \dot{w}_{5.1}}{N_f} \quad (\text{B49})$$

$$T'_{5.1} = T_5 \left[ 1.0 - \frac{\Delta h_{t2}}{(c_{p,t2} T_5)} \right] \quad (\text{B50})$$

$$c'_{p5.1} = \mathcal{F}_6 \left[ T'_{5.1}, \left( \frac{f}{a} \right)_5 \right] \quad (\text{B51})$$

$$\left( \frac{f}{a} \right)_5 = \frac{\left( \frac{f}{a} \right)_4}{1 + \left[ \left( \frac{f}{a} \right)_4 + 1 \right] \frac{\dot{w}_{b11}}{\dot{w}_5}} \quad (\text{B52})$$

$$\left( \frac{f}{a} \right)_{5.1} = \frac{\left( \frac{f}{a} \right)_5}{1 + \left[ \left( \frac{f}{a} \right)_5 + 1 \right] \frac{\dot{w}_{b12}}{\dot{w}_{5.1}}} \quad (\text{B53})$$

$$\gamma_{2.5} = \mathcal{F}_5(T_{2.5}, 0) \quad (\text{B54})$$

$$c_{p2.5} = \mathcal{F}_6(T_{2.5}, 0) \quad (\text{B55})$$

$$c_{v2.5} = c_{p2.5} / \gamma_{2.5} \quad (\text{B56})$$

$$\gamma_3 = \mathcal{F}_5(T_3, 0) \quad (\text{B57})$$

$$c_{p3} = \mathcal{F}_6(T_3, 0) \quad (\text{B58})$$

$$c_{v3} = \frac{c_{p3}}{\gamma_3} \quad (\text{B59})$$

$$\gamma_4 = \mathcal{F}_5 \left[ T_4, \left( \frac{f}{a} \right)_4 \right] \quad (\text{B60})$$

$$c_{p4} = \mathcal{F}_6 \left[ T_4, \left( \frac{f}{a} \right)_4 \right] \quad (\text{B61})$$

$$c_{v4} = \frac{c_{p4}}{\gamma_4} \quad (\text{B62})$$

$$\bar{T}_b = \beta_b T_3 + (1 - \beta_b) T_4 \quad (\text{B63})$$

$$c_{pb} = \mathcal{F}_6(\bar{T}_b, 0) \quad (\text{B64})$$

$$\gamma_5 = \mathcal{F}_5 \left[ T_5, \left( \frac{f}{a} \right)_5 \right] \quad (\text{B65})$$

$$c_{p5} = \mathcal{F}_6 \left[ T_5, \left( \frac{f}{a} \right)_5 \right] \quad (\text{B66})$$

$$c_{v5} = \frac{c_{p5}}{\gamma_5} \quad (\text{B67})$$

$$\gamma_{5.1} = \mathcal{F}_1 \left[ T_{5.1}, \left( \frac{f}{a} \right)_{5.1} \right] \quad (\text{B68})$$

$$c_{p5.1} = \mathcal{F}_2 \left[ T_{5.1}, \left( \frac{f}{a} \right)_{5.1} \right] \quad (\text{B69})$$

$$c_{v5.1} = \frac{c_{p5.1}}{\gamma_{5.1}} \quad (\text{B70})$$

$$\gamma_6 = \mathcal{F}_1 \left[ T_6, \left( \frac{f}{a} \right)_{5.1} \right] \quad (\text{B71})$$

$$c_{p6} = \mathcal{F}_2 \left[ T_6, \left( \frac{f}{a} \right)_{5.1} \right] \quad (\text{B72})$$

$$c_{v6} = \frac{c_{p6}}{\gamma_6} \quad (\text{B73})$$

$$N_f = \frac{30}{\pi I_f} \int_0^t (L_{t2} - L_f - L_{SC}) dt + N_{f,i} \quad (\text{B74})$$

$$N_c = \frac{30}{\pi I_c} \int_0^t (L_{t1} - L_c) dt + N_{c,i} \quad (\text{B75})$$

$$W_3 = \int_0^t (\dot{w}_3 - \dot{w}_{b11} - \dot{w}_{b12} - \dot{w}_{ovb} - \dot{w}_4) dt + W_{3,i} \quad (\text{B76})$$

$$T_3 = \int_0^t \frac{1}{W_3} \left\{ \frac{c'_{p3} T'_3 \dot{w}_3}{c_{v3}} - T_3 [\dot{w}_3 + (\gamma_3 - 1)(\dot{w}_4 + \dot{w}_{b11} + \dot{w}_{b12} + \dot{w}_{ovb})] \right\} dt + T_{3,i} \quad (\text{B77})$$

$$P_3 = \frac{R_A W_3 T_3}{V_3} \quad (\text{B78})$$

$$W_4 = \int_0^t (\dot{w}_4 + \dot{w}_F - \dot{w}_5) dt + W_{4,i} \quad (\text{B79})$$

$$T_4 = \int_0^t \frac{1}{W_4} \left\{ \frac{(c_{pb} \bar{T}_b \dot{w}_4 + \eta_b HVF \dot{w}_F)}{c_{v4}} - T_4 [\dot{w}_4 + \dot{w}_F + (\gamma_4 - 1) \dot{w}_5] \right\} dt + T_{4,i} \quad (\text{B80})$$

$$P_4 = \frac{R_A W_4 T_4}{V_4} \quad (\text{B81})$$

$$W_5 = \int_0^t (\dot{w}_5 + \dot{w}_{b11} - \dot{w}_{5.1}) dt + W_{5,i} \quad (\text{B82})$$

$$T_5 = \int_0^t \frac{1}{W_5} \left\{ \frac{(c'_{p5} T_5 \dot{w}'_5 + c_{p3} T_3 \dot{w}_{b11})}{c_{v5}} - T_5 [\dot{w}_5 + \dot{w}_{b11} + (\gamma_5 - 1)W_{5.1}] \right\} dt + T_{5,i} \quad (\text{B83})$$

$$P_5 = \frac{R_A W_5 T_5}{V_5} \quad (\text{B84})$$

$$W_{5.1} = \int_0^t (\dot{w}_{5.1} + \dot{w}_{b12} - \dot{w}_6) dt + W_{5.1,i} \quad (\text{B85})$$

$$T_{5.1} = \int_0^t \frac{1}{W_{5.1}} \left\{ \frac{(c'_{p5.1} T'_{5.1} \dot{w}'_{5.1} + c_{p3} T_3 \dot{w}_{b12})}{c_{v5.1}} - T_{5.1} [\dot{w}_{5.1} + \dot{w}_{b12} + (\gamma_{5.1} - 1)\dot{w}_6] \right\} dt + T_{5.1,i} \quad (\text{B86})$$

$$P_{5.1} = \frac{R_A W_{5.1} T_{5.1}}{V_{5.1}} \quad (\text{B87})$$

$$W_6 = \int_0^t (\dot{w}_6 - \dot{w}_8) dt + W_{6,i} \quad (\text{B88})$$

$$T_6 = \int_0^t \frac{1}{W_6} \left\{ \frac{c_{p5.1} T_{5.1} \dot{w}_6}{c_{v6}} - T_6 [\dot{w}_6 + (\gamma_6 - 1)\dot{w}_8] \right\} dt + T_{6,i} \quad (\text{B89})$$

$$P_6 = \frac{R_A W_6 T_6}{V_6} \quad (\text{B90})$$

$$W_{2.5} = \int_0^t (\dot{w}_{2.5} - \dot{w}_{2.8}) dt + W_{2.5,i} \quad (\text{B91})$$

$$T_{2.5} = \int_0^t \frac{1}{W_{2.5}} \left\{ \frac{c'_{P_{2.5}} T'_{2.5} \dot{w}_{2.5}}{c_{v_{2.5}}} - T_{2.5} [\dot{w}_{2.5} + (\gamma_{2.5} - 1)\dot{w}_{2.8}] \right\} dt + T_{2.5,i} \quad (B92)$$

$$P_{2.5} = \frac{R_A W_{2.5} T_{2.5}}{V_{2.5}} \quad (B93)$$

$$\dot{w}_4 = \left( \frac{A g_c}{l} \right)_b \int_0^t (P_3 - P_4 - \mathcal{A}_b \dot{w}_4^2) dt + \dot{w}_{4,i} \quad (B94)$$

$$\dot{w}_6 = \left( \frac{A g_c}{l} \right)_{cd} \int_0^t (P_{5.1} - P_6 - \mathcal{A}_{cd} \dot{w}_6^2) dt + \dot{w}_{6,i} \quad (B95)$$

$$\dot{w}_F = \text{output from fuel control} \quad (B96)$$

$$\dot{w}_{b11} = A_{b11} \sqrt{\frac{g_c}{R_A}} \frac{P_3}{\sqrt{T_3}} \mathcal{F}_7(\gamma_3) \quad (B97)$$

$$\dot{w}_{b12} = A_{b12} \sqrt{\frac{g_c}{R_A}} \frac{P_3}{\sqrt{T_3}} \mathcal{F}_7(\gamma_3) \quad (B98)$$

$$\dot{w}_{ovb} = A_{ovb} \sqrt{\frac{g_c}{R_A}} \frac{P_3}{\sqrt{T_3}} \mathcal{F}_7(\gamma_3) \quad (B99)$$

$$\dot{w}_8 = A_8 \sqrt{\frac{g_c}{R_A}} \frac{P_6}{\sqrt{T_6}} \mathcal{F}_8 \left( \gamma_6 \frac{P_a}{P_6} \right) \quad (B100)$$

$$\dot{w}_{2.8} = A_{2.8} \sqrt{\frac{g_c}{R_A}} \frac{P_{2.5}}{\sqrt{T_{2.5}}} \mathcal{F}_8 \left( \gamma_{2.5} \frac{P_a}{P_{2.5}} \right) \quad (B101)$$

$$\mathcal{F}_7(\gamma) = \sqrt{\gamma \left( \frac{2}{\gamma + 1} \right)^{\gamma+1/\gamma-1}} \quad (\text{B102})$$

$$\left. \begin{aligned} \mathcal{F}_8(\gamma, pr) &= \mathcal{F}_7(\gamma) \text{ if } pr \leq 0.53685 \\ &= (pr)^{1/\gamma} \sqrt{\frac{2\gamma}{(\gamma-1)} [1 - pr^{\gamma-1/\gamma}]} \text{ if } pr > 0.53685 \end{aligned} \right\} \quad (\text{B103})$$

$$F_8 = \dot{w}_8 \sqrt{c_{p6} T_6 \frac{2J}{g_c}} \mathcal{F}_9 \left( \gamma_6 \frac{P_{s,8}}{P_6} \right) + A_8 (P_{s,8} - P_a) \quad (\text{B104})$$

$$F_{2.8} = \dot{w}_{2.8} \sqrt{c_{p2.5} T_{2.5} \frac{2J}{g_c}} \mathcal{F}_9 \left( \gamma_{2.5} \frac{P_{s,2.8}}{P_{2.5}} \right) + A_{2.8} (P_{s,2.8} - P_a) \quad (\text{B105})$$

$$F_{\text{tot}} = F_{2.8} + F_8 \quad (\text{B106})$$

$$\left. \begin{aligned} P_{s,8} &= 0.53685 P_6 \text{ if } P_a/P_6 \leq 0.53685 \\ &= P_a \text{ if } P_a/P_6 > 0.53685 \end{aligned} \right\} \quad (\text{B107})$$

$$\left. \begin{aligned} P_{s,2.8} &= 0.53685 P_{2.5} \text{ if } P_a/P_{2.5} \leq 0.53685 \\ &= P_a \text{ if } P_a/P_{2.5} > 0.53685 \end{aligned} \right\} \quad (\text{B108})$$

$$\mathcal{F}_9(\gamma, pr) = \sqrt{1 - pr^{\gamma-1/\gamma}} \quad (\text{B109})$$

Fuel control:

$$y_1 = \text{MIN} \left\{ \begin{aligned} &K_4 (N_{f, \text{dem}} - N_{f, m}) \\ &K_5 (N_{c, \text{max}} - N_{c, m}) \end{aligned} \right\} \quad (\text{B110})$$

$$y_2 = \frac{1}{\tau_1} \int_0^t (K_{AV} \dot{x}_v - y_2) dt \quad \text{for } y_2 \leq 0.8 \quad (\text{B111})$$

$$y_3 = K_3(y_1 - y_2) \quad (\text{B112})$$

$$y_4 = K_{AC} \left( \sqrt{\frac{\varphi_{\min} P_{3,m}}{K_{mv}}} - x_v \right) \quad (\text{B113})$$

$$y_5 = \text{MAX} \left\{ \begin{array}{c} y_3 \\ y_4 \end{array} \right\} \quad (\text{B114})$$

$$y_6 = K_{AC} \left( \sqrt{\frac{\varphi_{\max} P_{3,m}}{K_{mv}}} - x_v \right) \quad (\text{B115})$$

$$y_7 = \text{MIN} \left\{ \begin{array}{c} y_5 \\ y_6 \end{array} \right\} \quad (\text{B116})$$

$$\dot{x}_v = K_V y_7 \quad (\text{B117})$$

$$x_v = \int_0^t \dot{x}_v dt + x_{v,i} \quad \text{for } 0.2 \leq x_v \leq 1.0 \quad (\text{B118})$$

$$\dot{w}_F = K_{mv} x_v^2 \quad (\text{B119})$$

$$\varphi_{\max} = \mathcal{F}_{10}(N_{c,m}, N_{f,m}) \quad (\text{B120})$$

$$\varphi_{\min} = \mathcal{F}_{11}(\varphi_{\max}) \quad (\text{B121})$$

Airplane roll control:

$$N_{f,dem} = N_{f,dem,\alpha} + N_{f,dem,\theta} \quad \text{for } 0.7 N_{f,100} \leq N_{f,dem} \leq N_{f,100} = N_{f,des} \sqrt{\frac{T_2}{T_{2,des}}} \quad (\text{B122})$$

$$N_{f,dem,\alpha} = N_{f,des}(\alpha) \sqrt{\frac{T_2}{T_{2,des}}} \quad \text{for } 0 \leq \alpha \leq 1.0 \quad (\text{B123})$$

$$N_{f,dem,\theta} = \sqrt{\frac{T_2}{T_{2,des}}} [K_1(g_{dem} - \theta) - K_2\dot{\theta}] \quad (\text{B124})$$

$$\ddot{\theta} = K_\theta \frac{n_{E^rAP}}{I_{AP}} (F - F_i) \quad (\text{B125})$$

$$\dot{\theta} = \int_0^t \ddot{\theta} dt \quad (\text{B126})$$

$$\theta = \int_0^t \dot{\theta} dt \quad (\text{B127})$$

$$\ddot{X} = K_X \frac{n_{E^rF_i} g_c \sin \theta}{W_{AP}} \quad (\text{B128})$$

$$\dot{X} = \int_0^t \ddot{X} dt \quad (\text{B129})$$

$$X = \int_0^t \dot{X} dt \quad (\text{B130})$$

## REFERENCES

1. Hill, T. Gardner: An All Turbofan VTOL or STOL Intercity Transport. *J. Aircraft*, vol. 8, no. 4, Apr. 1971, pp. 254-257.
2. Fry, Bernard L.; and Zabinsky, Joseph M.: Feasibility of V/STOL Concepts for Short-Haul Transport Aircraft. NASA CR-743, 1967.
3. Lieblein, S.: A Review of Lift-Fan Propulsion Systems for Civil VTOL Transports. Paper 70-670, AIAA, June 1970.
4. Kutney, J. T.: Propulsion System Development for V/STOL Transports. *J. Aircraft*, vol. 3, no. 6, Nov.-Dec. 1966, pp. 489-497.
5. Dugan, James F., Jr.; Krebs, Richard P.; Civinskas, Kestutis C.; and Evans, Robert C.: Preliminary Study of an Air-Generator-Remote Lift Fan Propulsion System for VTOL Transports. NASA TM X-67916, 1971.
6. Sanders, Newell D.; Diedrich, James H.; Hassell, James L.; Hickey, David H.; Luidens, Roger W.; and Stewart, Warner H.: V/STOL Propulsion. *Aircraft Propulsion*. NASA SP-259, 1971, pp. 135-168.
7. Shapiro, Ascher H.: *The Dynamics and Thermodynamics of Compressible Fluid Flow*. Vol. I. Ronald Press Co., 1953.
8. Seldner, Kurt; Mihaloew, James R.; and Blaha, Ronald J.: Generalized Simulation Technique for Turbojet Engine System Analysis. NASA TN D-6610, 1972.
9. Anderson, Seth B.: A Discussion of the Use of Thrust for Control of VTOL Aircraft. Integration of Propulsion Systems in Airframes. AGARD Conf. Proc. No. 27, Sept. 1967, pp. 6.1-6.9.

NATIONAL AERONAUTICS AND SPACE ADMINISTRATION  
WASHINGTON, D.C. 20546

OFFICIAL BUSINESS  
PENALTY FOR PRIVATE USE \$300

SPECIAL FOURTH-CLASS RATE  
BOOK

POSTAGE AND FEES PAID  
NATIONAL AERONAUTICS AND  
SPACE ADMINISTRATION  
451



POSTMASTER: If Undeliverable (Section 158  
Postal Manual) Do Not Return

*"The aeronautical and space activities of the United States shall be conducted so as to contribute . . . to the expansion of human knowledge of phenomena in the atmosphere and space. The Administration shall provide for the widest practicable and appropriate dissemination of information concerning its activities and the results thereof."*

—NATIONAL AERONAUTICS AND SPACE ACT OF 1958

## NASA SCIENTIFIC AND TECHNICAL PUBLICATIONS

**TECHNICAL REPORTS:** Scientific and technical information considered important, complete, and a lasting contribution to existing knowledge.

**TECHNICAL NOTES:** Information less broad in scope but nevertheless of importance as a contribution to existing knowledge.

**TECHNICAL MEMORANDUMS:** Information receiving limited distribution because of preliminary data, security classification, or other reasons. Also includes conference proceedings with either limited or unlimited distribution.

**CONTRACTOR REPORTS:** Scientific and technical information generated under a NASA contract or grant and considered an important contribution to existing knowledge.

**TECHNICAL TRANSLATIONS:** Information published in a foreign language considered to merit NASA distribution in English.

**SPECIAL PUBLICATIONS:** Information derived from or of value to NASA activities. Publications include final reports of major projects, monographs, data compilations, handbooks, sourcebooks, and special bibliographies.

**TECHNOLOGY UTILIZATION PUBLICATIONS:** Information on technology used by NASA that may be of particular interest in commercial and other non-aerospace applications. Publications include Tech Briefs, Technology Utilization Reports and Technology Surveys.

*Details on the availability of these publications may be obtained from:*

**SCIENTIFIC AND TECHNICAL INFORMATION OFFICE**

**NATIONAL AERONAUTICS AND SPACE ADMINISTRATION**

**Washington, D.C. 20546**